

# SUPERCONDUCTING PROPERTIES OF Be DOPED



## SUPERCONDUCTORS

BY

KEFAYAT ULLAH



Department of Physics  
Quaid-i-Azam University  
Islamabad, Pakistan.  
2010



# SUPERCONDUCTING PROPERTIES OF Be DOPED



## SUPERCONDUCTORS

A dissertation submitted to the department of physics, Quaid-i-Azam University Islamabad, in the partial fulfillment of the requirement for the degree of

*Master of Philosophy*

in

**Physics**

by

**KEFAYAT ULLAH**



Department of Physics  
Quaid-i-Azam University  
Islamabad, Pakistan.

2010





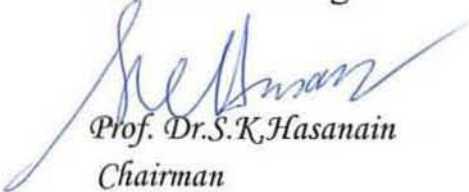
## Certificate

This is to certify that Mr. **Kefayat ullah s/o Sayed salar** has carried out the experimental work in this dissertation under my supervision in Materials Science Laboratory and is accepted in its present form by the Department of Physics, Quaid-i-Azam University Islamabad as satisfying the dissertation requirement for the degree of Master of Philosophy in Physics.

 Supervisor,

*Dr. Nawazish Ali Khan  
Department of Physics  
Quaid-I-Azam University  
Islamabad, Pakistan*

Submitted through:



*Prof. Dr. S.K. Hasanain  
Chairman*

*Department of physics  
Quaid-I-Azam University  
Islamabad, Pakistan.*

**Dedicated to my Brother**  
*Sayed atta-ullah* (late)  
**To whom these words may stand  
a little adoration.**

## ACKNOWLEDGEMENTS

Praise be to Thee! We do not know anything except what Thou hast made known to us: indeed Thou art the best Knower, the Wisest (Al-Quran).

My heart felt respects are for my Supervisor Dr. Nawazish Ali Khan, Associate Professor, Department of Physics, Quaid-i-Azam University Islamabad, for his affectionate devoted guidance, and for his unflinching support at all stages of this work.

I am highly obliged to Prof. Dr.S.K.Hasanain Chairman, Department of Physics, and Quaid-i-Azam University Islamabad, who is extremely supportive of all research activities.

My sincere regards and thanks are overdue to Sami Ullah, Sajid khan, and Muhammad Rahim for their constructive suggestions and technical guidance.

I am thankful to all my worthy colleagues, Dr. Najmul Hassan, Mr. M .Irfan, Hasnain, who bestowed me with their sincere and valuable suggestions.

Thanks are extended to M. Nawaz, Kamran, Saeed, Tariq, Salik, Yasir, Bilal, Khan Alam, Ibrahim, Zia Mashwani Faiq Jan, Hamid, Hayat, Hanif, and Meraj for their nice company during my M.Phil.

My humble and heartfelt gratitude is reserved for my beloved **Parents**, sisters and brothers. ZafarHayat, Arifullah, and Sayed Suliman Without their prayers, support and encouragement, the completion of this study task would have been a dream.



**KEFAYAT ULLAH**

## Abstract

We have enhanced the superconducting properties of newly discovered  $\text{Cu}_{0.5}\text{Tl}_{0.5}\text{Ba}_2\text{Ca}_1(\text{Cu}_{0.5}\text{Zn}_{1.5})\text{O}_{8-\delta}$  superconductor by doping Be at Ca sites. The superconducting properties, such as critical current density, infield magnetic properties and quantity of diamagnetism, are enhanced by Be doping at the Ca sites. The decreased c-axis length and the volume of the unit cell have shown that inter- $\text{ZnO}_2$ -plane coupling is enhanced. We have not observed any localization of the carriers in the neighbourhood of Zn atoms in  $\text{Cu}_{0.5}\text{Tl}_{0.5}\text{Ba}_2\text{Ca}_{1-y}\text{Be}_y(\text{Cu}_{0.5}\text{Zn}_{1.5})\text{O}_{8-\delta}$  ( $y=0, 0.15, 0.30, 0.45, 0.6$ ) superconductors, as proposed in the previous studies one must expect such effects if present, through the decreased c-axis length by Be doping. The decreased c-axis length results in enhancement of coherence length and Fermi-velocity of the carriers, which in turn result in enhanced superconductivity parameters. The presence of Be at the termination ends of the crystals results in enhanced inter-grain coupling and substantially improved their weak link behaviour. The optimization of the carriers in  $\text{CuO}_2/\text{ZnO}_2$ -planes have been found to enhance the  $T_c(R=0)$  and the magnitude of diamagnetism in Be-doped samples. Also the softening of phonon modes with the increased Be doping evidenced the incorporation of Zn at the  $\text{CuO}_2$  planar sites.





# Contents

## Introduction and Literature Review

Introduction .....	1
1.1 Historical Background.....	1
1.2 What is superconductor? .....	3
1.2.1 Zero resistivity.....	3
1.2.2 No magnetic induction ( $B = 0$ inside the superconductor).....	4
1.3 Types of superconductors.....	5
1.3.1 Type I and type II superconductors.....	5
1.4 BCS theory of superconductivity.....	6
1.5 Critical parameters .....	7
1.5.1 Critical Temperature.....	7
1.5.2 Critical Magnetic field.....	8
1.5.3 Critical current density .....	8
1.5.4 London penetration Depth .....	9
1.5.5 Coherence Length .....	9
1.6 High Temperature Superconductor .....	10
1.7 Structure of High Temperature Superconductors .....	11
1.8 Applications of superconductor .....	14
1.9 Literature Review .....	15
1.11 Motivation .....	19
References	

## Experimental Techniques

2.1	Sample Preparation .....	24
2.2	Post annealing of the sample.....	24
2.3	Characterization .....	25
2.3.1	XRD (X-ray Diffraction) .....	25
2.3.1(a)	X-ray Diffraction And Braggs law .....	25
2.3.1(b)	X-Ray Diffraction Method .....	27
2.3.1(c)	X-Ray Diffractometer .....	28
2.3.2	AC Magnetic Susceptibility .....	29
2.3.3	Resistivity measurements .....	30
2.3.4	Fourier transform infrared spectroscopy .....	32
2.3.5	References. ....	35

## Results and Discussion

3.1.	Introduction .....	36
3.2	Result and Discussion.....	37
3.3	Conclusions.....	56
3.4	References.....	57

## List of Figures

Figure 1.1	The plot of electrical resistance of mercury v/s Temperature.....	2
Figure 1.2	Temperature dependence of the resistivity of thin film of high-Tc superconductor YBa <sub>2</sub> Cu <sub>3</sub> O <sub>7</sub> .....	4
Figure 1.3	Expulsion of weak external magnetic field from the interior of the superconducting material.....	4
Figure 1.4	Magnetization v/s applied magnetic field for a type I superconductor. ....	5
Figure 1.5	Superconducting magnetization curve of a Type II superconductor. ....	6
Figure 1.6	Cooper pairs of electrons.....	7
Figure 1.7	Dependence of critical magnetic field of a superconductor on the temperature.....	8
Figure 1.8	(a) Structure of copper based 1223 high-Tc superconductor. (b) Structure of copper based 1234 high-Tc superconductor. (c) Structure of copper based 1245 high-Tc superconductor .....	12
Figure 1.9	Variation of Tc with number of CuO <sub>2</sub> Planes.....	13
Figure 2.1	Diffraction of X-Rays by planes of atoms .....	26
Figure 2.2	X-Ray Diffractometer .....	28
Figure 2.3	Experimental set up of ac-magnetic susceptibility measurements.....	30
Figure 2.4	Resistivity measurement setup.....	31
Figure 2.5	Basic diagram of Michelson interferometer.....	34
Figure 2.6	A schematic diagram of FTIR system.....	34
Figure 2.7	Vibrational modes of CO <sub>2</sub> molecules .....	34
Figure 3.1(a)	X-ray diffraction of (Cu <sub>0.5</sub> Tl <sub>0.5</sub> )Ba <sub>2</sub> Ca <sub>1-y</sub> Be <sub>y</sub> Cu <sub>0.5</sub> Zn <sub>1.5</sub> O <sub>8-δ</sub> (y= 0.0, 0.15, 0.30) Superconductors.....	38
Figure 3.1(b)	X-ray diffraction of (Cu <sub>0.5</sub> Tl <sub>0.5</sub> )Ba <sub>2</sub> Ca <sub>1-y</sub> Be <sub>y</sub> Cu <sub>0.5</sub> Zn <sub>1.5</sub> O <sub>8-δ</sub> (y= 0.45, 0.60) Superconductors.....	39
Figure 3.2	Variation of cell parameters v/s Be concentration.....	40
Figure 3.3a	Infrared absorption spectra of (Cu <sub>0.5</sub> Tl <sub>0.5</sub> ) Ba <sub>2</sub> Ca <sub>1-y</sub> Be <sub>y</sub> Cu <sub>0.5</sub> Zn <sub>1.5</sub> O <sub>8-δ</sub> (y=0.0, 0.15, 0.30) superconductor.....	42

Figure 3.3b	Infrared absorption spectra of $(\text{Cu}_{0.5}\text{Tl}_{0.5})\text{Ba}_2\text{Ca}_{1-y}\text{Be}_y\text{Cu}_{0.5}\text{Zn}_{1.5}\text{O}_{8-\delta}$ ( $y=0.45, 0.60, 0.75$ ) superconductor.....	43
Figure 3.3c	Oxygen-annealed infrared absorption spectra of $(\text{Cu}_{0.5}\text{Tl}_{0.5})\text{Ba}_2\text{Ca}_{1-y}\text{Be}_y\text{Cu}_{0.5}\text{Zn}_{1.5}\text{O}_{8-\delta}$ ( $y=0.0, 0.15, 0.30$ ) superconductor.....	44
Figure 3.3d	Oxygen-annealed infrared absorption spectra of $(\text{Cu}_{0.5}\text{Tl}_{0.5})\text{Ba}_2\text{Ca}_{1-y}\text{Be}_y\text{Cu}_{0.5}\text{Zn}_{1.5}\text{O}_{8-\delta}$ ( $y=0.45, 0.60, 0.75$ ) superconductor.....	45
Figure 3.4a	Resistivity measurements of $(\text{Cu}_{0.5}\text{Tl}_{0.5})\text{Ba}_2\text{Ca}_{1-y}\text{Be}_y\text{Cu}_{0.5}\text{Zn}_{1.5}\text{O}_{8-\delta}$ ( $y= 0.0, 0.15, 0.30, 0.45, 0.60,$ ) superconductor.....	47
Figure 3.4b	Transition region of the samples as prepared.....	47
Figure 3.5a	Oxygen-annealed Resistivity measurements versus temperature of $(\text{Cu}_{0.5}\text{Tl}_{0.5})\text{Ba}_2\text{Ca}_{1-y}\text{Be}_y\text{Cu}_{0.5}\text{Zn}_{1.5}\text{O}_{8-\delta}$ ( $y= 0.0, 0.15, 0.30, 0.45, 0.60,$ ) superconductors.....	49
Figure 3.5b	Transitions regions of the sample $\text{o}_2$ annealed.....	49
Figure 3.6a	Variation of $T_c$ with Be concentration.....	48
Figure 3.6b	Variation of $T_c$ with Be concentration of $\text{o}_2$ annealed sample.....	50
Figure 3.7	Resistivity of As prepared and $\text{O}_2$ Annealed $(\text{Cu}_{0.5}\text{Tl}_{0.5})\text{Ba}_2\text{Ca}_{1-y}\text{Be}_y\text{Cu}_{0.5}\text{Zn}_{1.5}\text{O}_{8-\delta}$ ( $y=0.75$ ) samples.....	51
Figure 3.8a	AC-susceptibility measurements versus temperature of $(\text{Cu}_{0.5}\text{Tl}_{0.5})\text{Ba}_2\text{Ca}_{1-y}\text{Be}_y\text{Cu}_{0.5}\text{Zn}_{1.5}\text{O}_{8-\delta}$ ( $y= 0.0, 0.15, 0.30, 0.45, 0.60,$ ) superconductors.....	53
Figure 3.8b	Oxygen-annealed AC-susceptibility measurements versus temperature of $(\text{Cu}_{0.5}\text{Tl}_{0.5})\text{Ba}_2\text{Ca}_{1-y}\text{Be}_y\text{Cu}_{0.5}\text{Zn}_{1.5}\text{O}_{8-\delta}$ ( $y= 0.0, 0.15, 0.30, 0.45, 0.60,$ ) superconductors.....	54
Table 1.1	A summary of onset of superconductivity $T_c(\text{onset}), T_c(R=0)$ in resistivity measurements and the onset of diamagnetism in In phase component of magnetic susceptibility and peak temperature in out phase component.....	55

# CHAPTER#1

## Introduction & literature review

Superconductivity is a fascinating and challenging field of physics. Scientist and engineers throughout the world have been striving to develop an understanding of this remarkable phenomenon for many years. Now a day's superconductivity is being applied to many diverse areas such as medicine, military, transportation, power production, electronics as well as many other areas.

### 1.1 Historical Background

Major advances in low temperature refrigeration were made during the 19<sup>th</sup> century. Superconductivity was first discovered in 1911 by the Dutch physicist, Heike Kammerlingh Onnes. On 1908 he successfully liquefied helium by cooling it to 4 Kelvin. Onnes produced only a few millilitres of liquid helium that time, but this was to be the new beginnings of his exploration in temperature regions previously unreachable. Liquid helium enabled him to cool other materials closer to absolute zero temperature.

In 1911, Onnes began to investigate the electrical properties of metals in extremely cold temperature. It had been known for many years that the resistance of metals fall when cooled below room temperature, but it was not known what limiting value the resistance would approach, if the temperature were reduced very close to zero K. Some scientists such as William Kelvin believed that electrons flowing through a conductor would come to a complete halt as the temperature was reduced to absolute zero. Other scientist, including Onnes, thought that a cold wire resistance would dissipate, this suggested that there would be a decrease in electrical resistance, allowing for better conduction of electricity. At some very low temperature, scientist expected that there would be a levelling off, as the resistance reached its minimum value allowing the current to flow with little or no resistance. Onnes passed a current through a very pure mercury wire and measured resistance as he steadily lowered the temperature. Much to his surprise there was no levelling off of resistance, let alone the stopping of electrons as suggested by Kelvin. At 4.2 Kelvin the resistance suddenly vanished. Current was flowing through the wires and nothing was stopping it, the resistance

drop to zero, Fig 1.1. According to Onnes “mercury has passed to a new state, which on account of its extraordinary properties may be called the “superconducting” state Onnes called this newly discovered state, superconductivity. In one of Onnes experiment, He started a current flowing through a loop of lead wire cooled to 4K. One year later the current was still flowing without significant current loss. Onnes found that the superconductor exhibited what he called persistent current i.e. Electric current that continued to flow without an electric potential driving them. Onnes was awarded with noble prize in 1913, for his discovery of superconductivity. [1]

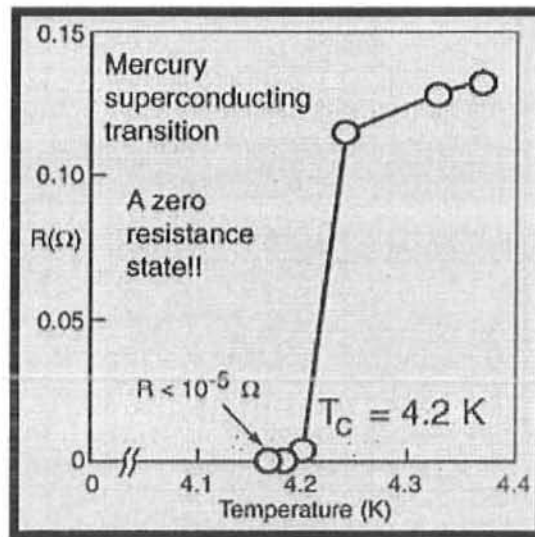


**Fig. 1.1** The plot shows the electrical resistance of mercury vs temperature [2].

In 1957 scientists began to unlock the mysteries of superconductors. Three American Physicists at the University of Illinois, John Bardeen, Leon Cooper, and Robert Schrieffer, developed a model that has since stood as a good mental picture of why superconductor behaves as they do. The model is expressed in terms of advanced ideas of the science of quantum mechanics, but the main idea of the model suggests that electrons in a superconductor condense into a quantum ground state and travel collectively and coherently. In 1972, Bardeen, Cooper, and Schrieffer received the Nobel Prize in Physics for their theory of superconductivity, which is now known as the BCS theory, after the initials of their last names [3].

## 1.2 What is a superconductor?

Superconducting materials have two fundamental properties:

### 1.2.1 Zero Resistivity

Zero resistivity, i.e. infinite conductivity, is observed in a superconductor at all temperatures below the critical temperature  $T_c$ , as depicted in Fig1.2. However, if the passing current is higher than the critical current  $J_c$ , superconductivity disappears. Why the resistivity of a superconductor is zero? If superconducting metal like Al or Hg is cooled below the critical temperature  $T_c$ , the gas of repulsive individual electrons that characterize the normal state transform itself into a different type of fluid, a quantum fluid of highly correlated pairs of electrons. A conduction electron of a given momentum and spin gets weakly coupled with another electron of the opposite momentum and spin. These pairs are called Cooper pairs. The coupling energy is provided by lattice elastic waves, called phonons. The behaviour of such a fluid of correlated Cooper pairs is different from the normal electron gas. They all move in a single coherent motion. A local perturbation, like an impurity, which in the normal state would scatter conduction electrons (and causes resistivity), cannot do so in the superconducting state without immediately affecting the Cooper pairs that participate in the collective superconducting state. Once this collective, highly coordinated, state of coherent super-electrons (Cooper pairs) is set into motion (like the super current induced around the loop), its flow is without any dissipation. There is no scattering of individual pairs of the coherent fluid and therefore no resistivity.

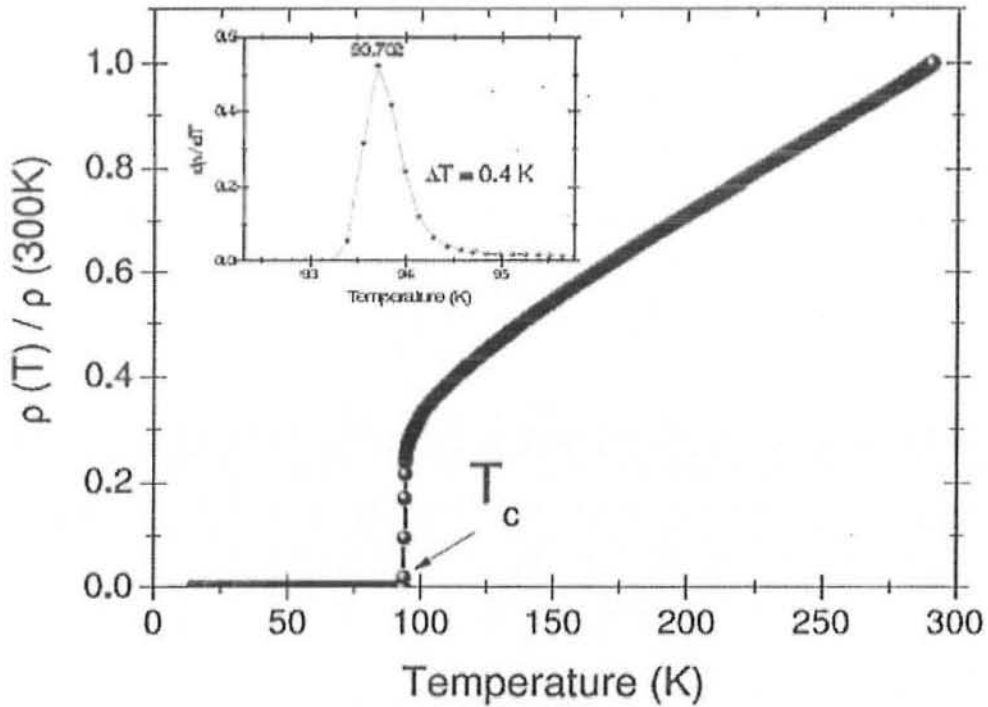


Fig. 1.2 Temperature dependence of the resistivity of a thin film of the high- $T_c$  Superconductor  $\text{YBa}_2\text{Cu}_3\text{O}_7$ ;

### 1.2.2 No magnetic induction ( $B = 0$ inside the superconductor)

In magnetic fields lower the critical field  $B_c$  the magnetic inductance becomes zero inside the superconductor when it is cooled below  $T_c$ . The magnetic flux is expelled from the interior of the superconductor see Fig.1.3. This effect is called the Meissner-Ochsenfeld effect after its discoverers. To test whatever a material is superconducting both properties  $\rho = 0$  and  $B = 0$  must be present simultaneously [4].

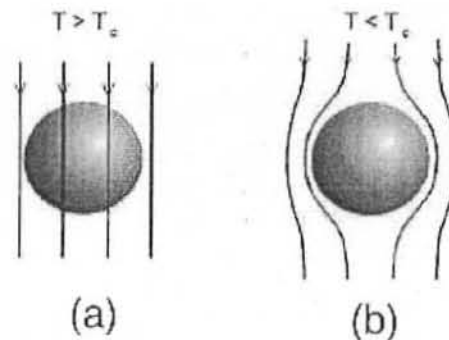


Fig. 1.3 Expulsion of a weak external magnetic field from the interior of the Superconducting material.



## 1.3 Types of Superconductors

There are two types of superconductors namely Type I and Type II superconductors. Existence of mixed state in type II superconductors differentiate between two types of superconductors. Type I superconductors can exist in one of its two states; superconducting or normal; where type II superconductor can exist in one of its three states i.e. superconducting, mixed or normal state [5].

### 1.3.1 Type I and type II Superconductors

There are traditionally, two types of superconductor. Type I superconductors are also called the 'soft' superconductors they are mostly the metals and metalloids that can conduct at normal temperatures. The elemental superconductors are called type I. The BCS theory explains these superconductors quite well. Noting their response to external magnetic field one can identify them.

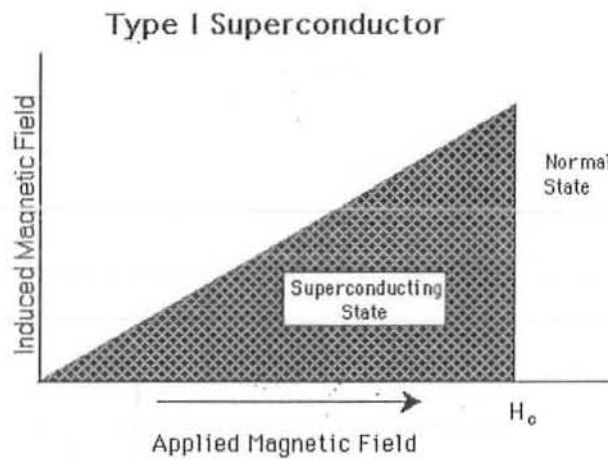


**Fig.1.4** Magnetization versus applied magnetic field for a type I superconductor.

The type I superconductor are those in which Meissner effect holds well. That is when the magnetic field is less than the critical magnetic field  $H_c$ , they expelled applied magnetic field  $B$  completely, see Figure 1.4, and when  $H$  become equal to or greater than  $H_c$ , superconductivity is destroyed and they become normal conductors. Type II superconductors, on the other hand are called the 'hard' materials, often have a higher  $T_c$  and  $H_c$ , but the

mechanism by which this occurs is still unknown. One of the main things differing in these materials from the type I superconductors is that in the presence of external magnetic field the transition from the normal to the superconducting range occurs over a transitional period, characterizing a 'mixed-state' during the transition. That is when magnetic field is increased from a value  $H < H_c$ , for some time the  $B$  inside remain zero till  $H$  reaches a value  $H_{c1}$ , during this period Meissner effect is complete. When the value of  $H$  increases beyond  $H_{c1}$ , then  $H$  begins to penetrate the superconductors, there are some regions which behave like normal material, and rest of regions are in superconducting state. As the field is increased further the number of normal region starts growing and  $H$  penetration increases till  $H$  becomes equal to  $H_{c2}$ , at that point the superconductivity is destroyed completely and sample becomes normal. Figure 1.5. The electrical properties of superconductor exist till  $H_{c2}$  the value of the  $H_{c2}$  may be 100 times or more high than the value of the  $H_{c1}$ , calculated from the thermodynamics of transition [6]

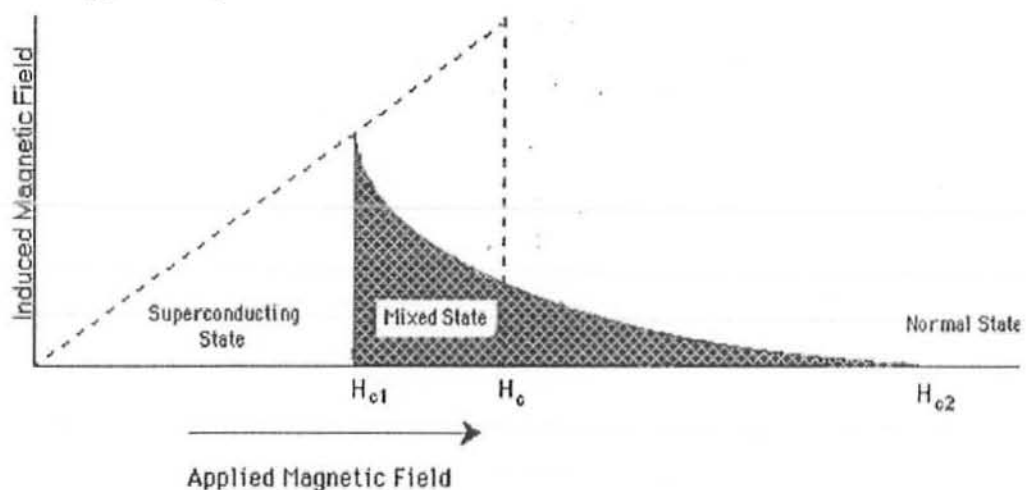
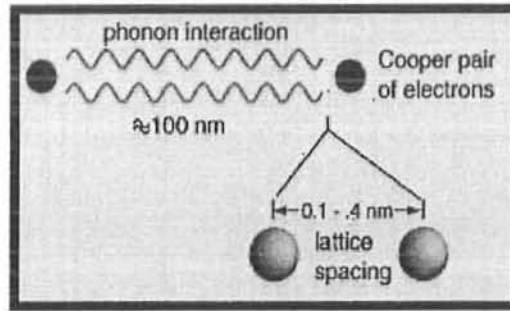


Fig.1.5. Superconducting magnetization curve of a Type II superconductor.

## 1.4 BCS Theory of Superconductivity

The properties of Type I superconductors were modeled successfully by the efforts of John Bardeen, Leon Cooper, and Robert Schrieffer in what is commonly called the BCS theory. A key conceptual element in this theory is the pairing of electrons close to the Fermi level into Cooper pairs through interaction with the crystal lattice. The electron pairs have a slightly lower energy and leave an energy gap above them on the order of .001 eV which

inhibits the kind of collision interactions which lead to ordinary resistivity. For temperatures such that the thermal energy is less than the band gap, the material exhibits zero resistivity [7].



**Fig. 1.6** Cooper pairs of electrons.

BCS theory starts from the assumption that there is some attraction between electrons, which can overcome the Coulomb repulsion. In most materials (in low temperature superconductors), this attraction is brought about indirectly by the coupling of electrons to the crystal lattice (as explained above). However, the results of BCS theory do not depend on the origin of the attractive interaction. The original results of BCS were describing an "s-wave" superconducting state, which is the rule among low-temperature superconductors but is not realized in many "unconventional superconductors", such as the "d wave" high temperature superconductors. Extensions of BCS theory exist to describe these other cases, although they are insufficient to completely describe the observed features of high temperature superconductivity. BCS were able to give an approximation for the attractive interaction of electrons inside the metal. This state is now known as the "BCS state". Whereas in the normal metal electrons move independently, in the BCS state they are bound into cooper pairs by the attractive interaction.

## 1.4 Critical Parameters

### 1.4.1 Critical Temperature

Superconducting alloys and metals have characteristic transition temperatures at which they are transformed from normal conductors to superconductors called critical temperatures ( $T_c$ ). According to BCS theory, as long as the superconductor is cooled to very low temperatures, the formation of cooper pairs takes place, due to the reduced atomic motion

(vibrations). As the superconductor gains heat energy, the vibrations in the lattice become more violent and break the pairs. As they break, superconductivity is destroyed. The resistivity of the material becomes zero below the superconducting critical transition temperature. Superconductors made from different materials have different  $T_c$  values [8].

### 1.4.2 Critical Magnetic Field

When a superconductor is cooled below its transition temperature ( $T_c$ ) and a magnetic field is increased around it. If we increase magnetic field to a certain point, the superconductor will go to the normal resistive state. This maximum value of the magnetic field (at a given temperature) is known as the critical magnetic field ( $H_c$ ). For all superconductors there exists a region of temperatures and magnetic fields with in which a material is in the superconducting state [8]. Outside this region, the material is in the normal state see Fig1.7

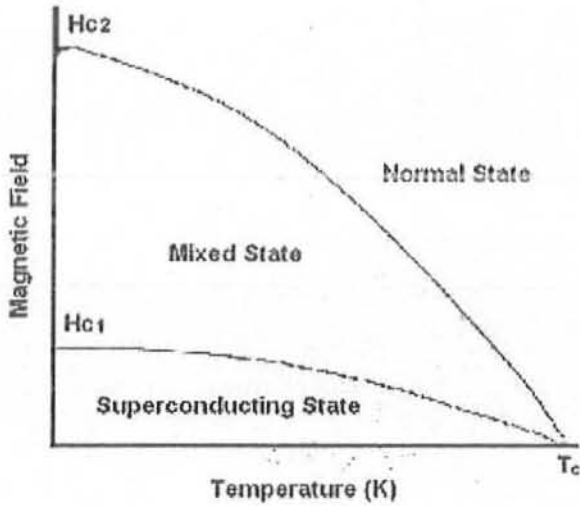


Fig.1.7 Dependence of critical magnetic field of a superconductor on the temperature.

### 1.4.3 Critical Current Density

There is a certain maximum current limit that the superconductors can carry, above which they become normal conductors. If too much current is pushed through a superconductor, it will revert to a normal state even though it may be below its transition

temperature and zero applied field. During  $J_c$  measurements it is observed that the colder you keep the superconductor the more current it can carry [9].

### 1.4.4 London Penetration Depth ( $\lambda$ )

In 1935, Fritz and Heinz London theoretically explained the Meissner effect by proposing two groups of electrons in a superconducting material, the superconducting electrons and the normal state electrons. They employed the Maxwell equations to develop a set of electrodynamics equations, called the London equations. According to the London equations, the magnetic field exponentially falls off with increasing distance from the surface of a superconducting sample. The characteristic decay length is called the London penetration depth ( $\lambda$ ), is given by

$$\lambda = (m_e / \mu_0 n_s e^2)^{1/2}$$

where  $m_e$  and  $e$  is the mass and charge of electron respectively,  $n_s$  is the number density of super-electrons. The temperature dependence of  $\lambda$  is given by empirical formula

$$\lambda_{(T)} = \lambda_{(0)} / [1 - (T/T_c)^4]^{1/2}$$

Where  $\lambda_{(0)}$  is the penetration depth at  $T=0$ , and is approximately equal to 60 nm for  $n_s$  about  $10^{22} \text{ cm}^{-3}$  [10].

### 1.4.5 Coherence Length ( $\xi$ )

According to BCS theory, despite the Coulomb repulsive forces between the electrons, due to distortion in the crystal structure (phonon mediation), slight attraction between pairs of electrons located near the Fermi surface leads to the production of bonded pairs of electrons, called Cooper pairs [11]. The size of a Cooper pair in a superconductor is known as the coherence length ( $\xi$ ). The BCS theory explained superconductivity in the low temperature and low magnetic field regime. Soon after that, the BCS theory was extended and became useful for high magnetic fields as well [12].

## 1.6 High temperature superconductors

After Onnes discovered superconductivity in 1911, many superconductors were discovered and the critical temperature rises year by year. The critical temperature of 22.3K was achieved in  $\text{Nb}_3\text{Ge}$ . After that, however, no higher temperature was obtained for more than 10 years. In 1986, revolution came in the field of superconductivity, when Bednorz and Muller discovered superconductivity in oxides of ceramic materials, i.e. La-Ba-Cu-O with a critical temperature of 30K [13]. The existence of demagnetization in this system was confirmed by magnetic studies. The critical temperature  $T_c(0)$  was found to increase by the replacement of Ba with Sr at normal pressure. It was also found that the application of external pressure increases the  $T_c(0)$  of the final compound. The possible source of increase of critical temperature is the reduction of lattice parameters and hence the unit cell volume under external pressure is applied [14].

In February 1987, Chu and others found a new superconducting material  $\text{YBa}_3\text{Cu}_3\text{O}_7$  with a critical temperature around 90K. Many scientists all over the world then began to search for new superconducting materials with higher critical temperatures. Structural analysis revealed that the lattice parameters of this compound follow orthorhombic structure. It was found through the detail characterization that Cu in the  $\text{CuO}_2$  planes was in mixed valance state; the average valancy of Cu in the plane is 2.2. The density of carrier of this orthorhombic phase in the conducting  $\text{CuO}_2$  planes controlled by  $\text{O}_2$  content in the chains, which play a vital role in achieving the superconductivity above 77K in this compound [14-15]. In spite of much effort, the reproducible superconductivity has remained at 90K for RE-Ba-Cu-O-based (RE = rare earth element) high temperature superconductors. Tremendous advances were made in theoretical and experimental research, and new materials were found in quick succession. Maeda, Sheng and Hermann made two important breakthroughs by their discoveries of superconductivity in Bi-based and Tl-based superconductors [16]. Maeda *et al* synthesized the Bi-Sr-Ca-Cu-O oxide, with transition temperature around 110K. These series of superconductors are more ductile and stable than La and Y-based superconductor because it consists of several superconductive phases, which are not trivial to be separated [17]. Another characteristic of CuO based high temperature superconductor Tl-Ba-Ca-Cu-O is the two superconducting phases, one with single Tl-O layer and the other with double Tl-O layer in

their charge reservoir block. These two compounds have critical temperature of 130K and 127K respectively. Due to their higher critical current  $J_c$ , and irreversibility field  $H_{irr}$  coupled with their lower surface resistance  $R_s$  made these compounds promising candidates in device fabrication and wire application. The Tl-based materials have also got multiphase character, which is controlled by amount of Tl and fabrication temperature [18].

A Superconducting system with even higher critical temperature belongs to Hg-Ba-Ca-Cu-O family have also been discovered. In Hg-based high temperature superconductors, the  $Hg_1Ba_2Ca_2Cu_3O_{8+\delta}$  has highest critical temperature around 135K, which is prepared at normal pressure. The Hg-based superconductors were also prepared under high pressure, which provided crucial clues to the existence of superconductivity at higher temperatures. The critical temperature of optimally doped phases  $HgBa_2Ca_{m-1}Cu_mO_{2m+2+\delta}$  with  $m=1, 2, 3$  have been investigated. The critical temperature of  $HgBa_2Cu_1O_{4+\delta}$  is 94K,  $Hg_1Ba_2Ca_1Cu_2O_{6+\delta}$  and  $Hg_1Ba_2Ca_2Cu_3O_{8+\delta}$  phase has shown  $T_c$  around 135K respectively. The  $T_c$  of later two phases has shown dependence on oxygen content in  $HgBa_2O_{4-\delta}$  charge reservoir layer. For Hg-based superconductor the highest  $T_c$  attained as up to now is 138K of  $Hg_{0.8}Tl_{0.2}Ba_2Ca_2Cu_3O_8$  phase. The resistivity of these compounds when measured under pressure have shown  $T_c(0)$  around 160K [19-20]. Another class of high temperature superconductor is  $CuBa_2Ca_{n-1}Cu_nO_{2n+4-\delta}$ , which has  $CuBa_2O_{4-\delta}$  charge reservoir layer. These materials have Cu lying in the charge reservoir layer and possessing the lowest anisotropy ( $\gamma=1.6$ ) among all cuprates high temperature superconductors. The highest  $T_c(0)$  in this family is credited to Cu-1223, with  $T_c(0) = 120K$ . These compounds are prepared under high pressure ( $\sim 4GPa$ ) [20-21]. The partial replacement of Cu by Tl in the charge reservoir made it possible, to synthesis these compound at normal pressure. The resulting  $Cu_{1-x}Tl_xBa_2Ca_{n-1}Cu_nO_{2n+4-\delta}$  compound still has low anisotropy and higher critical temperature. The  $Cu_{1-x}Tl_x$ -1223 compound of this family has  $T_c(0)$  around 132K, which is highest in this family [22].

## 1.7 Structure of High Temperature Superconductor

Multi layered cuprate have common structural characteristic described by the formula  $MCa_{n-1}Cu_nO_{2n}$ , where M is the Charge reservoir layer and  $Ca_{n-1}Cu_nO_{2n}$  are superconductor

block. The charge reservoir layer is generally represented by  $ABa_2O_{4-\delta}$ , where A: Tl, Bi, Cu, Hg. The type of atom 'A' in the charge reservoir layer forms a new homologous series of superconductor compound. Structures of different superconductors are shown in the Fig.1.9.

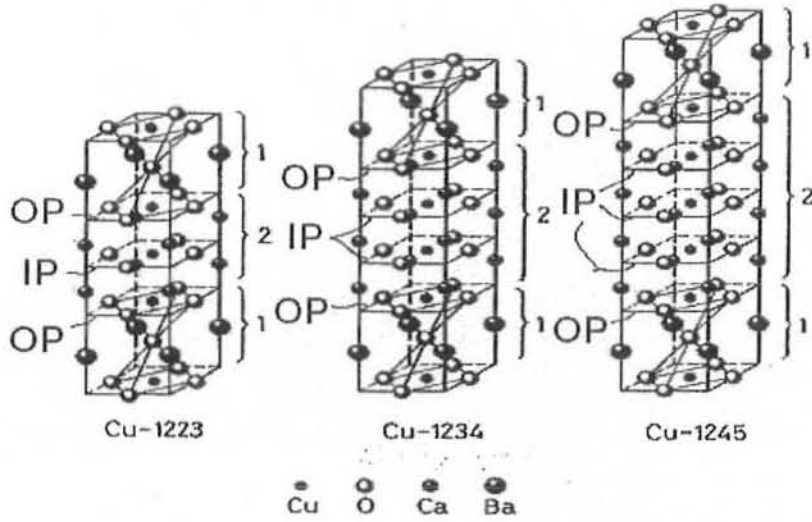


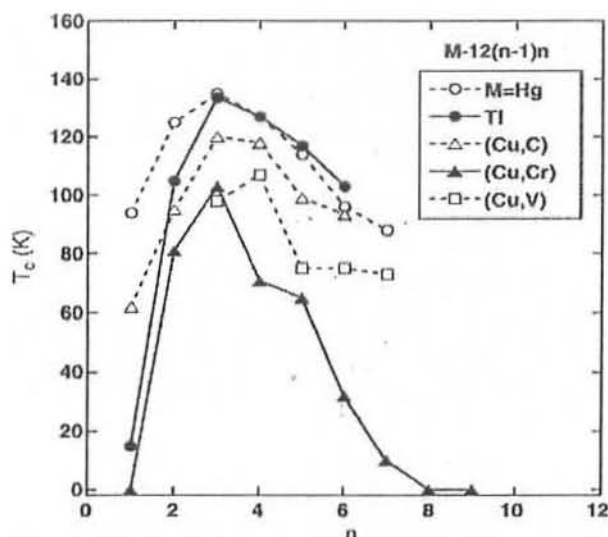
Fig.1.8

Fig.1.8 shows a model of a typical crystal structure of the copper-based high-temperature superconducting material consisting of carrier supply layer in block 1. The block 2 have two sets of planes (a) which are directly connected with the charge reservoir layer, outer planes (OP), (b) these planes are not connected with the charge reservoir layer and are called inner-planes (IP). In each homologous series the number of  $CuO_2$  planes varies from  $n=1, 2, 3, 4, 5$ . The function of charge reservoir layer is to supply the carriers to the conducting  $CuO_2$  planes and the optimum number of carriers in there, which determines the critical temperature of a particular compound. The outer planes are found over-doped with carriers, whereas the inner planes are in under doped region of carrier doping [23].

The number of planes of  $CuO_2$  planes has great influence on superconducting transition temperature in homologous series. The  $T_c(0)$  increases up to  $n=3$  and then decreases with further increase in  $n$ . It is suggested that the inhomogeneous distribution of carriers in inner and outer  $CuO_2$  planes is responsible for decrease in the  $T_c(0)$  for  $n>3$  so, the  $T_c(0)$  is determined from the intrinsic  $T_c$ 's of the two types of the  $CuO_2$  planes. Fig.1.9 Shows the



variation of critical temperature as a function of 'n' (number of CuO<sub>2</sub> planes) for typical multilayered cuprate of MBa<sub>2</sub>Ca<sub>n-1</sub>Cu<sub>n</sub>O<sub>2n</sub> (M=Hg, Tl) [24-25].



**Fig.1.9** Variation of  $T_C$  with number of CuO<sub>2</sub> planes

The charge distribution among the CuO<sub>2</sub> planes well correlates with the electrostatic potential associated with apical oxygen at each CuO<sub>2</sub> plane, which has more attraction for holes in the outer plane (OP) than in the inner plane (IP). The difference in the doping level increases with n, which increases the density of carriers. This difference between the  $N_h(OP)$  and  $N_h(IP)$  is smallest for  $n=3$  and the inner plane can achieve an optimally-doped state, that is the reason due to which most of the multilayered-cuprates have the highest  $T_C$  at  $n=3$ . It has been pointed out that the decrease in  $T_C$  for  $n \geq 4$  is due to the large inhomogeneity of the carrier distribution in various CuO<sub>2</sub> planes. The outer plane (OP) can have enough charge carriers for superconductivity, whereas the inner plane (IP) carriers become too small to induce superconductivity. Systematic investigation of the multilayered high- $T_C$  superconductor by nuclear magnetic resonance (NMR) experiments have shown that the carrier concentration of OP( $N_h$ ) adjacent to the charge reservoir layer (CRL) is always greater than that of IP( $N_h$ ) [25-26].

Since the discovery of superconductivity in both CuBa<sub>2</sub>Ca<sub>n</sub>Cu<sub>n+1</sub> and TlBa<sub>2</sub>Ca<sub>n</sub>Cu<sub>n+1</sub> systems such as Cu-12n(n+1) and Tl-12n(n+1) systems, their extensive characterization have been carried out. Both of these systems are isostructural except the position of oxygen in the

charge reservoir layer. Optimizing the carrier concentration could enhance the superconducting properties of these compounds. The carrier concentration could be control by cation substitution, by varying oxygen contents and by applying external pressure . The as-prepared samples of  $\text{CuTl-}12n(n+1)$  superconductors are in the region over doping of carrier and the density of state near the Fermi level  $D(E_F)$  is greater than optimum value. By carrying out post-annealing in nitrogen atmosphere, we can optimize the carrier concentration in  $\text{CuTl-}1223$  superconductor. The post-annealing experiments can increase the critical temperature of this compound. Through these experiments, we can optimize the charge state of Tl atoms from  $\text{Tl}^{+3}$  to  $\text{Tl}^{+1}$ . Thallium with  $\text{Tl}^{+1}$  has lower contents of oxygen with it, whereas  $\text{Tl}^{+3}$  has more oxygen. The more oxygen in the charge reservoir layer hinders the flow of electron to the conducting  $\text{CuO}_2$  planes; oxygen controls this through its higher electronegativity. The lower oxygen concentration associated with  $\text{Tl}^{+1}$  can efficiently allow the flow of electrons to the conducting  $\text{CuO}_2$  planes. Therefore, the change in oxidation state of the system brings the carrier concentration in  $\text{CuO}_2$  planes to the desired level [27].

On the other hand, the doping of various cations especially the alkali metals and transition metals at the planar site and at charge reservoir layer has a strong influence on the properties of high temperature superconductors [28].

## Applications:

Besides the scientific interest, the search for applications has always been a driving force for superconductor materials science [29]. Right from the discovery, it had been envisioned that SC coils with high persistent current might be used to generate strong magnetic fields. However, in the first generation of SC materials (.type-I.) superconductivity was easily suppressed by magnetic fields: The magnetic self-field generated by the injected current prevented high-field as well as high-current applications. A first step towards this goal was the discovery of type-II superconductors where the magnetic penetration depth  $\lambda$  exceeds the SC coherence length  $\xi$ . This enables a coexistence of superconductivity and magnetic fields, which are allowed to penetrate into the SC bulk in the quantized form of vortices. The concomitant substantial reduction of the loss of SC condensation energy that has to be paid for magnetic field penetration facilitates the survival of superconductivity even in strong

magnetic fields, at least up to a certain critical field  $H_{c2}$  where the SC state no longer survives the vortex Swiss cheesing.. The last ingredient required for technically applicable hard superconductors was the discovery and engineering of pinning centers which fix penetrated magnetic flux and prevent its Lorentz force driven flow through the superconductor that otherwise generates power dissipation.

Josephson junctions, well-defined weak links of SC regions, can be coupled to Superconducting Quantum Interferometric Devices. (.SQUIDs.) [30], magnetic flux detectors with quantum accuracy that are the most sensitive magnetic field detectors presently available. HTS SQUIDs at liquid nitrogen operation have approached this magnetic sensitivity within one order of magnitude [31] and are already in commercial use for the nondestructive evaluation (NDE) of defects in complex computer chips [32] and aircrafts. For all these applications of superconductivity, the necessity of cryogenics is at least a psychological burden. Nevertheless, with the present progress of small cryocoolers [33] SC devices may evolve within foreseeable future to push-button black-box machines that may be one day as common practice as nowadays vacuum tube devices in ordinary living rooms.

Superconductors are materials that lose their resistance to electrical current flow below a certain critical temperature ( $T_c$ ), a certain critical current density ( $J_c$ ) and certain critical field ( $H_c$ ). Superconductors have generated great interest for power applications including loss-free electric transmission cables, motors, generators, transformers, energy storages, levitation trains, ultra-fast computers etc. Besides that, the superconductivity phenomenon also opens the challenges to modern physics of superconductors [34].

## Literature review

E. Kandył *et al* [35] synthesized  $(Tl_{0.5}Pb_{0.5})Sr_2Ca(Cu_{2-x}M_x)O_7$  ( $M=Co, Ni$  and  $Zn$ ) superconductors and investigated by means of X-ray diffraction, scanning electron microscope, electrical resistivity and magnetic susceptibility measurements. X-ray diffraction patterns show that all studied samples contain the nearly single '1212' phase. They crystallize in a tetragonal unit cell with  $a=3.8028-3.8040\text{\AA}$  and  $c=12.0748-12.1558\text{\AA}$ . In  $(Tl_{0.5}Pb_{0.5})Sr_2Ca(Cu_{2-x}M_x)O_7$  system. The superconducting critical temperature  $T_c$  decreases linearly with both  $Co$  and  $Ni$  concentrations. For  $(Tl_{0.5}Pb_{0.5})Sr_2Ca(Cu_{2-x}Zn_x)O_7$  system, the dependence of  $T_c$  on the  $Zn$  dopant concentration deviates from a linear behaviour and the  $Zn$

substitution suppresses  $T_c$  much less than the Co and Ni substitutions. The suppression in  $T_c$  in Co and Ni doped samples are attributed to the magnetic pair-breaking mechanism and the reduction in the carrier concentration. The suppression of  $T_c$  in Zn doped samples is not caused by the reduction in carrier concentration which should remain constant, but rather due to nonmagnetic pair-breaking mechanism induced by disorder as well as the filling of the local Cu  $d_{x^2-y^2}$  state due to the full d band of Zn ions.

N.A Khan *et al* [36] studied the substitution of Be at Ca site at normal pressure synthesized the  $\text{Cu}_{0.5}\text{Tl}_{0.5}\text{Ba}_2\text{Ca}_{n-1}\text{Cu}_n\text{O}_{2n+4-\delta}$  ( $n=3,4$ ) superconductor. The primary goal in synthesizing Be substituted sample was improvement of inter-plane coupling. Predominant single phases of  $\text{Cu}_{0.5}\text{Tl}_{0.5}\text{Ba}_2\text{Ca}_{2-y}\text{Be}_y\text{Cu}_3\text{O}_{2n+4-\delta}$  ( $y=1.0,2.5$ ) and  $\text{Cu}_{0.5}\text{Tl}_{0.5}\text{Ba}_2\text{Ca}_{3-y}\text{Be}_y\text{Cu}_4\text{O}_{12-\delta}$  ( $y=1.5,2.0$ ) superconductors were prepared by solid state reaction method both of the batch of samples have zero resistivity critical temperature at 95K. Bulk superconductivity and zero resistivity critical temperature are confirmed by ac-susceptibility measurements.  $a$  and  $c$ -axes length decreases with increase concentration of Be in  $\text{Cu}_{0.5}\text{Tl}_{0.5}\text{Ba}_2\text{Ca}_{3-y}\text{Be}_y\text{Cu}_4\text{O}_{12-\delta}$  ( $y=1.5,2.0$ ) superconductor. The decreased  $c$ -axis length suggests the improved inter-plane coupling in  $\text{Cu}_{0.5}\text{Tl}_{0.5}\text{Ba}_2\text{Ca}_1\text{Be}_2\text{Cu}_4\text{O}_{12-\delta}$  ( $y=1.5,2.0$ ) superconductors. The increased inter-plane coupling is also evidenced in FTIR absorption measurements.

K. Tomimoto *et al* [37] studied the impurity effects on the superconducting coherence length in Zn or Ni-doped  $\text{YBa}_2\text{Cu}_3\text{O}_{6.9}$  single crystals. They reported that coherence length ( $\xi$ ) increased along both the in-and out-of-plane directions. They suggested that the doped impurities acted as pair breakers. They concluded that increased coherence length ( $\xi$ ) along both the in-and out-of-plane directions could be well explained by the pair-breaking theory of  $d$ -wave superconductivity and the modification in the inter-plane coupling of the order parameter due to the presence of impurities

Y. X. Zhou *et al* [38] investigated the effect of ionic doping on the superconducting properties of  $\text{YBa}_2(\text{Cu}_{1-x}\text{M}_x)_3\text{O}_{7-\delta}$  ( $M = \text{Co}, \text{Ni}, \text{Zn}, \text{and Ga}$ ) due to their closer ionic size and similar outer orbital to that of Cu when they are substituted for Cu ions at Cu(1) and Cu(2) sites of the Cu-O chains and  $\text{CuO}_2$  planes respectively. The doping of Zn and Ni shows high  $T_c$  suppression as compared to the doping of Co and Ga. As Zn and Ni go to the Cu(2) site, while the Co and Ga substitute Cu(1) chain site. The trapped field at the pinning centre and their

population increases the levitation forces and enhancement in the  $J_c$ . Such effects are highest in Zn doped sample.

The effects of Co and Zn doping on the magnetization of  $\text{Bi}_{2.1}\text{Sr}_{1.8}\text{Ca}(\text{Cu}_{1-x}\text{M}_x)_2\text{O}_y$  ( $M = \text{Co}$ , and Zn) have been studied by X. R. Zhao *et al* [39] They found that a smaller amount of Zn below  $x=0.005$  is useful to enhance  $H_m(T)$  and  $J_c$  without severe reduction of  $T_c$ . The effect of Zn doping on the structure shows different change in the values of a- and b-axes resulting in transformation from tetragonal to orthorhombic structure. Resistive measurements show the increased scattering centers in the Zn doped Bi-2212 crystals as compared to undoped one.

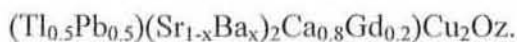
Goto *et al* [40] investigated the effects of Zn on Tl-1212 phases by NMR and noticed that the suppression rate in the transition temperature for over-doped region is lower than that for optimum-doped samples. They also found that the reduction rate of  $T_c$  in Tl-1212 samples was lower than that found in LSCO and YBCO.

A. Crisan *et al* [41] doped Cu-1234 with various concentrations (up to 2%) Zn tentatively on the Cu-site in the  $\text{CuO}_2$  superconducting planes, creating the pinning centers. Single phase samples with the composition of  $(\text{Cu M})\text{Ba}_2\text{Ca}_3\text{Cu}_4\text{O}_y$  (CuM-1234;  $M = \text{C}$ , Al, Mg, Zn, and Ni) have been synthesized using high pressure technique and measured the pressure dependence of superconducting transition temperature  $T_c$  through resistivity measurements up to 8 GPa. Shows the pressure dependence of  $T_c(K)$  for various CuM-1234 samples. They also carried out the transport, magnetic measurements and their iodometric titration analysis for oxygen contacts determination. The substitution of Zn at Cu site in superconducting  $\text{CuO}_2$  planes of CuM-1234 superconductor possibly brings about the reduction of  $T_c$ . The  $T_c$  suppression for Zn doped cuprate superconductors has been explained by magnetic pair breaking effect due to the appearance of Cu spin. A selective doping mechanism indicates an over-doped situation for the outer two  $\text{CuO}_2$  planes connected with the apical oxygen and nearly the optimal doping for inner two  $\text{CuO}_2$  layers. It is felt, that in such a scenario Zn might occupy the outer most  $\text{CuO}_2$  planes and not affect the  $T_c$ , as observed. The relative sensitivity of the charge reservoir layer towards pressure may be gauged by Al, Tl and high Cu-content materials, which occupy the vacancies present in the charge reservoir layer.

O. Chmaissem *et al* [42] successfully synthesized a new (Hg,V)-based 1212-type cuprate  $(\text{Hg}_{1-x}\text{V}_x)\text{Sr}_2(\text{Y}_{1-y}\text{Ca}_y)\text{Cu}_2\text{O}_z$  The electrical resistance measurements showed that

some of the as-synthesized materials with proper Hg/V and Y/Ca ratios exhibit weak superconductivity. Oxygen-annealing significantly improved their superconducting behavior, and  $T_{\text{conset}}$  up to 110 K was observed. Then lattice parameters of (Hg,V)-1212 were found to be in the order of  $a=3.8415 \text{ \AA}$  and  $c=11.8514 \text{ \AA}$ . Substituting mercury atoms by vanadium ones results in an important increase of the  $a$  parameter and an important decrease of the  $c$  parameter compared to the known Hg based Sr-bearing compounds. The crystal structure of (Hg, V)-1212 was refined by Rietveld refinement against X-ray powder data using the tetragonal symmetry of space group  $P4/mmm$ .

G. Gritzner *et al* [43] synthesised Thallium-free precursors for bulk superconductors with the overall composition  $(\text{Tl}_{0.5}\text{Pb}_{0.5})(\text{Sr}_{1-x}\text{Ba}_x)_2(\text{Ca}_{1-y}\text{Gd}_y)\text{Cu}_2\text{O}_z$  ( $x = 0.0, 0.05, 0.1, 0.15, 0.2, 0.25, y = 0.0, 0.05, 0.1, 0.2, 0.3, 0.4$ ) were prepared via wet chemical gel techniques. The respective amounts of  $\text{Tl}_2\text{O}_3$ ,  $\text{PbO}$  and  $\text{Gd}_2\text{O}_3$  were co-milled to the precursor and the mixture was subjected to a heat treatment first at  $850 \text{ }^\circ\text{C}$  followed by sintering at  $925 \text{ }^\circ\text{C}$  in order to optimize the superconducting properties of the bulk material. X-ray diffraction showed that samples with  $x$  and  $y$  equal to or smaller than 0.2 were nearly phase-pure. While changes in the  $x$  value had little effect on the properties of the materials, a Gd stoichiometry of 0.2 yielded the best results in this series. Critical temperatures around 100 K were obtained for samples with the composition



A. Ehmann [44] *et al* studied Bi cuprate of type 1212 and synthesized above  $970 \text{ }^\circ\text{C}$  from the proper starting material. The oxides of idealized composition  $(\text{Bi}_{0.5}\text{Cu}_{0.5}\text{Sr}_2\text{YCuO}_{7-z})$  crystallize in the tetragonal space group  $P4/mmm$  ( $a=3.815 \text{ \AA}$ ,  $c= 11.73 \text{ \AA}$  and show solid solution behaviour. The as-prepared materials are non-superconducting above 5 K. However, post-treatment in flowing oxygen at moderate temperature of  $500 \text{ }^\circ\text{C}$  introduces superconductivity. The highest superconducting transition temperature is situated at 68 K for a sample of nominal composition  $(\text{Bi}_{0.5}\text{Cu}_{0.5}) - \text{Sr}_2\text{Y}_{0.8}\text{Cu}_{2.2}\text{O}_{6.95}$ .

P. Halder *et al* [45] characterized high  $T_c$  superconductor containing thallium  $(\text{Tl}_{0.75}\text{Bi}_{0.25}) \text{Sr}_{1.33}\text{Cu}_2\text{O}_{6.67+\delta}$  with ideal stoichiometry  $\text{Tl,Bi}1\text{Sr}_2\text{Ca}_1\text{Cu}_2\text{O}_{6.5+\delta}$ . As prepared sample have shown an initial deviation of resistance from linearity at 120K a superconducting onset temperature of 92 k and zero resistance at 75K. These sample have shown tetragonal structure with  $a=3.800 \text{ \AA}$   $c=12.07 \text{ \AA}$ , deduced from powder data.

G.c.che, *et al* [46] studied 1212 type (Pb,Cd) based cuprate superconductor system  $(\text{Pb}_{0.5}\text{Cd}_{0.5})\text{Sr}_2(\text{Tl}_{1-x}\text{Ca}_x)\text{Cu}_2\text{O}_7$  has been prepared in tetragonal lattice cell parameter  $a=3.822\text{\AA}$   $c=11.95\text{\AA}$  and space group  $p_4/mmm$ . For  $x=0$  the sample exhibited bulk superconductivity with a transition temperature of 19K.

## Motivation

$\text{CuBa}_2\text{Ca}_{n-1}\text{Cu}_n\text{O}_{2n+4-\delta}$  [Cu-12(n-1)n];  $n = 1, 2, 3, \dots$ , samples are thought to be the most promising due to their higher critical temperature  $T_c(R=0)$ , critical current density  $J_c$  and lower anisotropy. The lower anisotropy consequently enhances their technological critical temperature ( $Z=T_c/\gamma$ ), irreversibility field ( $H_{ir} = H_{c2}/\gamma$ ) and critical current density. But the main problem associated with this family, which makes its large-scale production difficult, is the high pressure (4-6 GPa) synthesis method. However, by introducing thallium into the charge reservoir layer of Cu-12(n-1)n, the superconducting phases  $\text{Cu}_{1-x}\text{Tl}_x\text{-12(n-1)n}$  are obtained by normal pressure synthesis. These compounds are prepared under high as well as normal pressure and have superconducting properties very close to Cu-12(n-1)n compounds. The members of this new family have semi insulating charge reservoir layer  $\text{Cu}_{1-x}\text{Tl}_x\text{Ba}_2\text{O}_{4n-\delta}$  that slightly increases their anisotropy but its value still remains lower than the Tl-12(n-1)n compounds. One-way of reducing the superconducting anisotropy is to improve the inter-plane couplings and in the presents studies, it will be done by substituting smaller size Be at Ca sites. The superconducting properties of these compounds may further be enhanced by post annealing and by substitution of different cations.

The existence of superconductivity in  $(\text{Cu}_{0.5}\text{Tl}_{0.5})\text{Ba}_2\text{Ca}_{n-1}\text{Zn}_n\text{O}_{2n+4-\delta}$  ( $n=3,4$ ) superconductors with  $\text{ZnO}_2$  planes [47] is preferred over its parent compound  $(\text{Cu}_{0.5}\text{Tl}_{0.5})\text{Ba}_2\text{Ca}_{n-1}\text{Cu}_n\text{O}_{2n+4-\delta}$  ( $n=3,4$ ) with  $\text{CuO}_2$  [48], due to the fixed valance state of zinc which can introduce a material with uniform carrier density in the inner and outer planes. In the later compound existence of anti-ferromagnetism is witnessed in the inner  $\text{CuO}_2$  planes. The anti-ferromagnetic alignment of spins of  $3d^9$  Cu atoms is suggested to arising from the deficiency of the carriers there; the outer planes and over-doped whereas the inner planes are under-doped with the carriers. The existence of anti-ferromagnetism in the IP of  $\text{MBa}_2\text{Ca}_{n-1}\text{Cu}_n\text{O}_{2n+4-\delta}$  ( $M=\text{Bi, Tl, Hg, Cu}$ ) superconductors has been found to suppress the critical temperature and magnitude of diamagnetism [49]. Another advantage a superconductor with  $\text{ZnO}_2$  planes with filled  $3d^{10}$  shell is suppression of local spin density which was being induces by Cu  $3d^9$  shell in the  $\text{CuO}_2$  planes and

hence the interactions of spins with the free carriers in Zn-doped compounds is significantly reduced. It has also been observed from our studies that hundred percent Zn cannot replace the Cu atoms in  $(\text{Cu}_{0.5}\text{Tl}_{0.5})\text{Ba}_2\text{Ca}_{n-1}\text{Zn}_n\text{O}_{2n+4-\delta}$  ( $n=3,4$ ) and a solubility limit appears with 90% Zn doping at the Cu sites; with the doping of Zn beyond this limit superconductivity disappears altogether. These observations lead us to a conclusion that some population of Cu  $3d^9$  atoms is essential in the  $\text{CuO}_2/\text{ZnO}_2$  planes for the accomplishment of charge transfer from the charge reservoir layer. Another suggestion arising out of these observations is existence of interactions of spin density wave with the charge density wave as proposed in the charge stripe model [50]. The ideal compound for such studies is two [51-52]  $\text{CuO}_2/\text{ZnO}_2$  planes plane  $\text{Cu}_{0.5}\text{Tl}_{0.5}\text{Ba}_2\text{Ca}_1\text{Cu}_{0.5}\text{Zn}_{1.5}\text{O}_{8-\delta}$  superconductor, because the under-doped inner-planes would be absent altogether in this compound.

In our previous studies we have a develop a better correlation among the carriers in  $\text{ZnO}_2$  planes, by doping Mg at the Ca sites in  $(\text{Cu}_{0.5}\text{Tl}_{0.5})\text{Ba}_2\text{Ca}_{n-1}\text{Zn}_n\text{O}_{2n+4-\delta}$  ( $n=3,4$ ) superconductors, consequently enhanced superconductivity is achieved. It was observed from the studies of the cell parameters of Mg doped compounds that volume of the unit cell decreases resulting in increase in the Fermi vector  $[K_F=(3\pi^2N/V)^{1/3}]$ , their coherence length  $[\xi_c=h^2K_F/2m\Delta]$  along c-axis and hence the Fermi velocity  $[V_F = \frac{\pi\xi_c\Delta}{\eta}]$  [53] of the carriers. In order to observe the above effects we have doped Be at the Ca sites in  $(\text{Cu}_{0.5}\text{Tl}_{0.5})\text{Ba}_2(\text{Ca}_{1-y}\text{Be}_y)(\text{Cu}_{0.5}\text{Zn}_{1.5})\text{O}_{8-\delta}$  ( $y=0, 0.15, 0.3, .45, 0.6, 0.75$ ) superconductors. The main objective of this to enhance the inter-plane coupling and increase the interactions of remaining Cu atoms spins with the carriers in the conducting  $\text{ZnO}_2/\text{CuO}_2$  planes. These experiments would help in understanding charge density wave and spin density wave and the role of their interaction in the mechanism of high temperature superconductivity.



## References:

- [1] *Materials Science*, M.S.Vijaya and G Rangarajan, Tata McGraw-Hill Publishing Company Limited New Delhi (2004).
- [2] Kammerlingh Onnes, H. Comm. Physical Lab. Leiden 133d 51 (1913).
- [3] *Solid State Physics*, M.Ali Omer Pearson education (Singapore) Pte ltd Indian branch 482 F.I.E Delhi India.
- [4] Soltan Eid Abdel-Gawad Soltan. Interaction of Superconductivity and Ferromagnetism in YBCO/LCMO Heterostructures. Dissertation, Max-Planck- Institute Fuer Festkoerperforschung, 2005.
- [5] *Materials Science*. Rajendran, A. Marikani, Tata McGraw-Hill Publishing Company Limited, New Delhi (2004).
- [6] *Superconductivity, Super fluid and Condensate*, James F. Annet, First Edition, Oxford University Press, (2003).
- [7] *Introduction to Superconductivity*, Michael Tinkham, McGraw-Hill.Inc, New York 1996.
- [8] *Solid State Physics and Electronics*,R.K Puri and V.K Babbar,(1997).
- [9] *Introduction to Superconductivity*, A.C.Rose -Innes and E.H Roderick second Edition,(1976).
- [10] F. London and H. London, Proc. Roy. Soc. A **149** 71-88. (1935).
- [11] L.N. Cooper, Physical Review, **104**, 1189-1190. (1956).
- [12] L.P.Gorkov, Soviet Physics JETP **10** 998-1004 (1960).
- [13] J. G. Bednorz and K. A. Muller, Z. Phys. B, Vol **64** p.189, (1986).
- [14] C. W. Chu, P. H. Hor, R. L. Meng, Phys. Rev. Lett. **58**, 9 (1987).
- [15] A. G. Mamalis, D. E. Manolakos, A. Szalay, G. Pantazopoulos, Processing of High Temperature Superconductor, Penneclvenia 17604 U.S.A, 2000.
- [16] Z. Sheng, W. Kiehl, J. Bennett, Phys. Rev. Lett. **52**, 20 (1988).
- [17] L. Gao, Y. Y. Xue, F. Chen, Q. Xiong, Phys. Rev B. **50**, 6 (1994).
- [18] H. Ihara, K. Tanaka, A. Iyo, N. Terada, Physica B**1085**, (2000).

- [19] K. Tokiwa, H. Aota, A. Iyo, Phys B. 1077-1078 (2000).
- [20] T. Watanabe, S. Miyashita, N. Ichioka, Phys B **1075** (2000).
- [21] A. Iyo, Y. Tanaka, Y. Kodama, H. Kito, Physica C 445-448 (2006).
- [22] Xiaojia Chem, Changde Gong, Phys. Rev. B, **59**, 6 (1999).
- [23] K. Tanaka, A. Iyo, N. Terada, Phys Rev B. Vol. **63**,064508 (2001).
- [24] S.Isber, R Awad, Supercond Sci. Technol. **18** 311-316 (2005).
- [25] Robert V. kasowski, Phys. Rev B vol. **38**, No. 10 (1998).
- [26] K. Tanaka, A. Iyo, N. Terada, Phys Rev B. Vol. **63**,064508 (2000).
- [27] Y. Tanaka, H. Ihara, N. Terada, Phys B. **284-288** (2000).
- [28] *High Temperature Superconductivity Engineering Applications* (Ed. A. V. Narlikar), Springer Verlag, Berlin (2004).
- [29] *Superconductivity Fundamentals and Applications* W. Buckel, R. Kleiner, WILEY-VCH Verlag, Weinheim (2004).
- [30] *Dynamics of Josephson Junctions and Circuits*, K. K. Likharev, Gordon & Breach Science Publishers, (1986).
- [31] *SQUID Handbook* (Ed. J. Clarke, A. Braginski), WILEY-VCH Verlag, Berlin (2003).
- [32] *High Temperature Superconductivity 2 -Engineering Applications* D. Koelle, R. Kleiner, F. Ludwig, E. Dantsker, J. Clarke, Rev. Mod. Phys. **71** (1999). 631,H. J. Barthelmeß, F. Ludwig, M. Schilling, D. Drung, T. Schurig (Ed. A. V. Narlikar), Springer Verlag, Berlin, (2004).
- [33] L. A. Knauss, A. B. Cawthorne, N. Lettsome, S. Kelly, S. Chatrathorn, E. F. Fleet, F. C. Wellstood, W. E. Vanderlinde, Microelectronics Reliability **41**1211 (2001).
- [34] *High Temperature Superconductivity 2 - Engineering Applications*, M.v.Kreutzbruck, (Ed. A. V. Narlikar), Springer Verlag, Berlin, (2004).
- [35] E. Kandyela, M.A. Sekkinaa, M.A.T. Dawoudb and M.Y. Bonham, Solid State Commun. **135** 214 (2005).
- [36] N. A. Khan, and G. Husnain, K.Sabeah. Journal of physics and chemistry of solids 436 **51** (2006).
- [37] K. Tomimoto, I. Terasaki, A. I. Rykov, T. Mimura and S. Tajima Phys. Rev. B **60** 114 (1999).
- [38] Y. X. Zhou, S. Scruggs, and K. Salama, Supercond. Sci. Technol. **19**, S556 (2006).

- [39] X. R. Zhao, K. Kitazawa, and T. Hasegawa, *Physica C* **370**, 44-52 (2000).
- [40] T. Goto, S. Nakajima, M. Kikuchi, and T. Fukase, *Physica C* **263**, 8750 (1997).
- [41] A. Crisan, S. K. Agarwal, T. Koganezawa, R. Kuroda, K. Tokiwa, T. Watanabe, A. Iyo, Y. Tanaka, and H. Ihara, *J. Phys. Chem. Solids* **63**, 1073-1076 (2002).
- [42] Chmaissem, Z.Z. Sheng *Z. Phys. B* **99**, 179D184 (1996).
- [43] G.Gritzner, H.Sudra and M.Eder, *Journal of Physics: Conference Series* **43** 462-465(2006).
- [44] A. Ehmanna, S. Kemmler-Sacka, S. L.Ssch a, M. Schlichenmaier, W. Wischerta, Zoller a, T. Nissel b and R.P. Huebener b *PhysicaC* **198**1-6 (1992).
- [45] P.H halder, *Journal of Superconductivity*, vol 1 no,2 1988.
- [46] G che et al *Physica C* **251** 110-114 (1995).
- [47] B. A. Scott, E. Y. Suard, C. C. Tsuei, D. B. Mitzi, T. R. McGuire, B. -H. Chen, and D. Walker, *Physica C* **230** 239. (1994).
- [48] E. V. Antipov, A. M. Abakumov, and S. N. Putilin, *Supercond. Sci. Technol.* **15** R31(2002).
- [49] M. Núñez-Regueiro, and C. Acha, *Studies on High T<sub>c</sub> Superconductors*, Vol. **24**, Nova Science, Commack, NY, (2000).
- [50] M. -H. Julien, P. Carretta, M. Horvatic, C. Berthier, Y. Berthier, P. Segransan, A. Carrington, and D. Colson, *Phys. Rev. Lett.* **76** 4238(1996).
- [51] Y. Tokunaga, K. Ishida, Y. Kitaoka, K. Asayama, K. Tokiwa, A. Iyo and H. Ihara, *Phys.Rev. B* **61**, 9707 (2000).
- [52] O. Zachar, S. A. Kivelson, and V.J. Emery, *Phys. Rev. B* **57**, 1422 (1998).
- [53] *Solid State Physics: An introduction to Theory and Experiment*, H. Ibach, H. Luth, first ed., Springer Velag, Berlin, P128 1993.

## CHAPTER#2

### Experimental Techniques

#### 2.1 Preparation

The superconductor samples of  $\text{Cu}_{0.5}\text{Tl}_{0.5}\text{Ba}_2\text{Ca}_{1-y}\text{Be}_y\text{Cu}_{0.5}\text{Zn}_{1.5}\text{O}_{8-\delta}$  ( $y=0, 0.15, 0.30, 0.45, 0.60, 0.75$ ), were prepared by solid state reaction method. The precursor material of  $\text{Cu}_{0.5}\text{Ba}_2\text{Ca}_{1-y}\text{Be}_y\text{Cu}_{0.5}\text{Zn}_{1.5}\text{O}_{8-\delta}$  was prepared using  $\text{Cu}(\text{CN})$ ,  $\text{Ba}(\text{NO}_3)_2$ ,  $\text{Ca}(\text{NO}_3)_2$ ,  $\text{ZnO}$ ,  $\text{BeO}$  as starting compounds. These compounds were mixed according to above mentioned formula unit for one hour in a quartz mortar and pestle. Thoroughly mixed material was put in a quartz boat and loaded into a preheated box furnace at  $825^\circ\text{C}$ . The mixed material was fired twice for 24 hours following intermediate grinding. The fired precursor material was mixed with a calculated amount of  $\text{Tl}_2\text{O}_3$  to give  $\text{Cu}_{0.5}\text{Tl}_{0.5}\text{Ba}_2\text{Ca}_{1-y}\text{Be}_y\text{Cu}_{0.5}\text{Zn}_{1.5}\text{O}_{8-\delta}$  as final reactants composition. The pellets of thallium mixed material were prepared under  $3.8\text{tons}/\text{cm}^2$  pressure. The pellets were enclosed in a gold capsule and sintered at  $825^\circ\text{C}$  for 10 minutes. The superconductor samples were characterized by resistivity measurements by four-probe method and structure was determined by XRD (X-ray diffraction) and FTIR (Fourier Transform Infrared Spectroscopy) absorption measurements.

#### 2.2 Post-Annealing of the Samples

The oxygen in oxide superconductors can modify the distribution of the carriers in various bands of a compound the electronic distribution ultimately controls the process of superconductivity. The post-annealing of the superconductor samples in oxygen and nitrogen atmospheres can increase or decrease the oxygen concentration in the materials. Therefore, we carried out post-annealing of  $\text{Cu}_{0.5}\text{Tl}_{0.5}\text{Ba}_2\text{Ca}_{1-y}\text{Be}_y\text{Cu}_{0.5}\text{Zn}_{1.5}\text{O}_{8-\delta}$  superconductor samples in oxygen atmosphere at  $500^\circ\text{C}$  for 5 hours in a preheated tubular furnace followed by furnace cooling to the samples to room temperature after the heat treatment.

## 2.3 Characterization

The samples were characterized by the following techniques

2.3.1) X-ray diffraction

2.3.2) AC susceptibility measurements

2.3.3) Resistivity measurements

2.3.4) Fourier Transform Infrared (FTIR) Spectroscopy

In this section a brief theoretical background and the description of the experimental setup for above-mentioned characterizations will be given

### 2.3.1 X-Ray Diffraction

XRD (X-ray diffraction) analysis gives us the information about the crystal structure of the material. This technique is used to know whether the intended sample has the crystalline structure or not and also to know the unit cell parameters.

#### X-Ray Diffraction and Bragg's law

Scattering of the waves with the closely spaced obstacles is called diffraction. Scattering can occur from obstacles only when the spacing between two obstacles is comparable to the wavelength of the wave. Furthermore, diffraction is a consequence of specific phase relationships between two or more waves that have been scattered from closely spaced obstacles. X-rays are electromagnetic waves with high energies and wavelengths of the order of the atomic spacing for solids. When a beam of X-rays is incident on a solid material, a portion of this incoming beam is scattered in all directions by the electrons of atoms or ions that lies in the path of the beam. The strong diffracted x rays are observed only in those directions in which the phases of the all scattered waves are the same. If the scattered waves are out of phase with one another then no diffraction is observed in that direction.

In order to understand the necessary conditions for the diffraction of x-rays from a periodic arrangement of atoms, consider three parallel planes of atoms. These planes have same Miller indices i.e.  $h$ ,  $k$  and  $l$ . The spacing between parallel planes " $d_{hkl}$ ". Now if a parallel, monochromatic and coherent (in phase) beam of x-rays of wavelength  $\lambda$  falls on these three planes at an angle  $\theta$ , then the three rays in the beam will be scattered by the three atoms located at the positions A, C and E in the three planes as shown in Fig.2.1

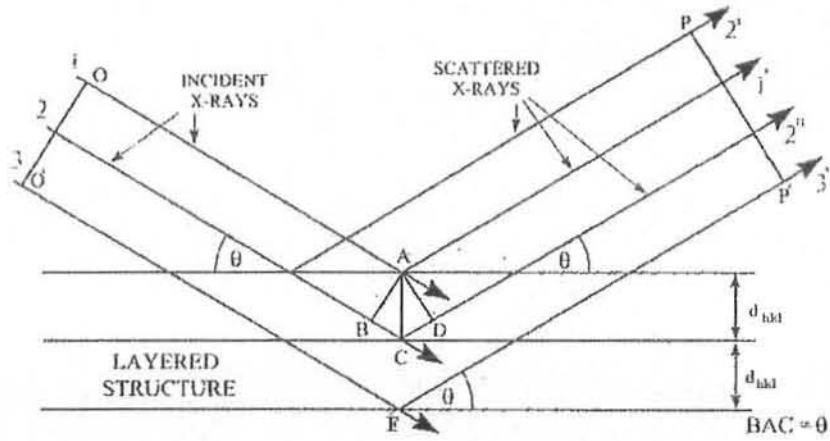


Fig. 2.1. Diffraction of x-rays by planes of atoms.

It is obvious that all these three waves travel along different path lengths, hence when they reach at point P they could be in phase if the path difference between them is integral multiple of the wavelength, i.e.

$$n \lambda = 2 d_{hkl} \sin \theta \quad (2.1)$$

Where 'n' is the order of diffraction, which may be any integer, i.e.  $n=1,2,3\dots$

This is known as the Bragg's Law. For a fixed value of ' $\lambda$ ' and ' $d_{hkl}$ ' there may be several values of angles of incidence  $\theta_1, \theta_2, \theta_3$  etc. from which the diffraction may occur for the corresponding 'n' values. If the Bragg law is satisfied then the waves interfere constructively and in the end one gets a high intensity waves as diffraction pattern. Otherwise the waves will interfere destructively and no diffracted beam will be observed. Hence we can say that the Bragg law is necessary condition for diffraction. Since  $\sin \theta$  cannot exceed unity, we may write equation (2.1)

as,

$$n\lambda / 2d_{hkl} = \sin \theta < 1 \quad (2.2)$$

Therefore,  $n\lambda$  must be less than  $2d_{hkl}$ . For diffraction the smallest value of 'n' is 1. The  $n=0$  corresponds to the beam diffracted in the same direction as the transmitted beam, so it cannot be observed. Therefore, the condition for diffraction at any observable angle is

$$\lambda < 2d_{hkl} \quad (2.3)$$

For most set of crystal planes ' $d_{hkl}$ ' is of the order of  $3\text{\AA}$  or less, which means that  $\lambda$  can not exceed about  $6\text{\AA}$  [1].

Bragg's law is necessary but not sufficient condition for diffraction from real crystals. It specifies that the diffraction will occur for unit cells having atoms positioned only at cell corners. However, atoms situated at other sites (e.g. face and interior unit cell positions such as with FCC and BCC) act as extra scattering centers, which can produce out of phase scattering at certain Bragg's angles. The net result is the absence of some diffracted beams that according to equation 2.1 should be present.

### X-Ray Diffraction Methods

It is evident that diffraction will occur only if wavelength of incoming beam of x-ray and angle of orientation of planes are in requirement with Bragg's law. This is very difficult to satisfy in practice hence various techniques have been developed to overcome the difficulty possessed by the Bragg's law. Few of these techniques are given as under [2].

	Wavelength ( $\lambda$ )	Angle of diffraction ( $\theta$ )
1) Lau Method	Variable	Fixed
2) Rotating Crystal Method	Fixed	Variable
3) Powder Method	Fixed	Variable

The powder method is also called as Debye - Scherer; this method is suitable for materials when a perfect single crystal is not available. Finely grained polycrystalline material, with individual crystallites of the order of micron, is placed in the path of the incoming x-rays. Because small crystals are present in all orientations in the sample, the net effect is same as a single rotating crystal experiment that turns the crystal through all possible directions, and there is a ring of scattering peaks corresponding to every reciprocal lattice vector of magnitude less than the twice of the incoming beam [3]. Since our samples are polycrystalline, therefore, we employ powder diffraction method. The specimen consisting of many fine and randomly oriented particles are exposed to monochromatic x-rays, which give the high-resolution diffraction pattern.

## X-Ray Diffractometer

The Diffractometer is represented schematically in Fig. 2.2. A powder specimen in the form of a flat plate is supported so that rotation about the axis is possible; this axis is perpendicular to the plane of paper. The monochromatic x-ray is generated in x-ray tube and is passed through a divergent slit to produce a well-defined focused beam. The beam then hit the powder specimen and the intensities of the diffracted beams after passing through the receiving slit are detected with a counter. The specimen, x-ray source and counter are all coplanar. The counter is mounted on moveable carriage that may also be rotated about its axis; its angular position in the term of  $2\theta$  is calculated on a marked scale. The carriage and the specimen are mechanically arranged in such a way that a rotation of the specimen through angle  $\theta$  is accompanied by a  $2\theta$  rotation of the counter, this assure that the incident and reflection angle are maintained equal to one another. Utilization of a filter provides a near monochromatic beam. As the counter moves at constant angular velocity, a recorder automatically plots the diffracted beam intensity (monitored by the counter) as function of  $2\theta$ .

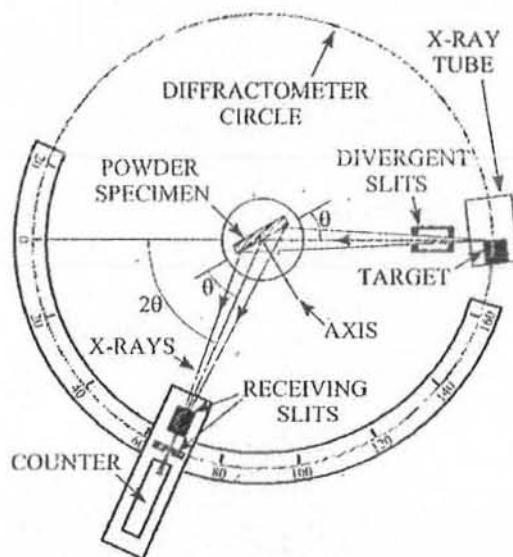


**Fig. 2.2** An x-ray Diffractometer.

Once the scattered peaks data is obtain then the data is analyzed for the determination of the crystal structure. The process proceeds in stages. The first step is to compare the location of the peaks/rings with those produced by the various known crystal structures and effort is made to identify the crystal structure. Next step is refinement procedure; varying locations of atoms and intensities of the species best fitting data is obtained. In our work we



used computer software “Check cell” which when provided with peak data, identified the crystal structure and also provide lattice parameters.

### 2.3.2 AC Magnetic Susceptibility

Magnetic susceptibility is a measure of the sample magnetization due to the external applied magnetic field [4].

Mathematically

$$\chi = \frac{M}{H}$$

In ac susceptibility measurements the sample, magnetic response is checked by a sensing change of its magnetization in a coil produced by varying ac magnetic field i.e.

$$\chi = \frac{dM}{dH_{ac}} \quad (2.4)$$

In AC measurements the moment of the sample changes in response to an applied AC field. This dynamical behavior of the magnetic system shows the frequency dependence of the complex susceptibility. AC susceptibility probes the entire volume of the sample and provides the magnetic response of sample in volume fraction (i.e. superconducting and normal volume fractions). The AC susceptibility technique has been used to determine the onset of diamagnetism at which a normal material goes into superconducting state. This is the transition between a complete magnetic field shielding and the onset of magnetic flux penetration inside a superconducting sample. In magnetic measurements, the susceptibility has two parts (real and imaginary part). The real part of susceptibility ( $\chi'$ ) represents the magnitude of diamagnetic shielding currents to the external AC magnetic field. The loss component or imaginary part ( $\chi''$ ) of the complex susceptibility represents the coupling between the grains. In an external applied magnetic field the peak in the imaginary part of the susceptibility is defined as the onset of the irreversibility. For a complete Meissner expulsion ' $\chi'$ ' is negative, and for a full flux penetration ' $\chi'$ ' is zero. Similarly for a complete superconducting state ' $\chi''$ ' is zero while in the mixed superconducting state ' $\chi''$ ' is positive number reflecting AC losses.

We have used the AC susceptometer based on mutual induction method. The AC susceptometer consists of two coils, one is a primary coil which is used to induce emf in to secondary coil consisting of two parts wound opposite directions so that the flux in one secondary coil is exactly equal and opposite to the flux in the second part of it. The sample is placed in lower part of secondary coil. In the normal state there is no output signal. When the sample is in superconducting state, the diamagnetic signal of the sample it cancels the flux of the coil in which sample is place which results in off-balancing of the coil; the magnitude of which shows the strength of superconductivity in a sample. The voltage of the off-balancing of the coil is feed in a lock-in-amplifier and the signal is separated into real and imaginary parts. The ac susceptibility setup is shown in the form of a block diagram in Fig.2.3

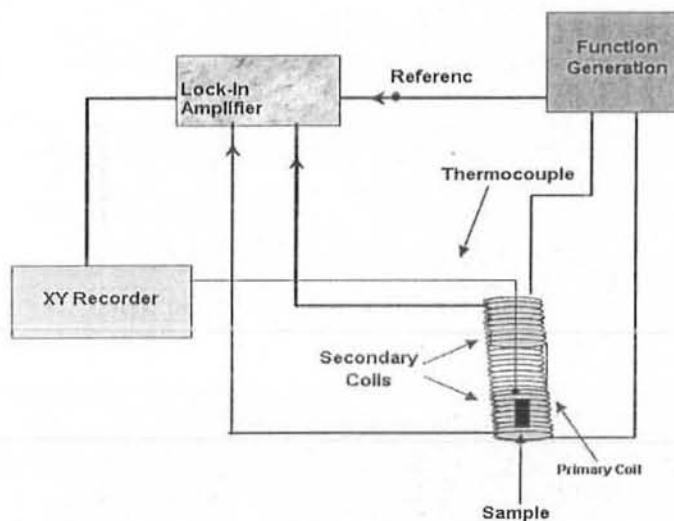


**Fig.2.3** Experimental set up of ac-magnetic susceptibility measurements.

### 2.3.3 Resistivity measurements

The resistivity measurements of a superconductor are used to find out the critical temperature  $T_c(R=0)$  and the onset temperature of superconductivity  $T_c(\text{onset})$  as well as their normal state properties. The sources of resistivity in the normal state would be the scattering of electrons from the defects in the lattice, lattice vibrations and electron-electron collisions [5]. The electron-electron scattering is negligible as compared to electron-defect and electron-phonon scattering. So the resistivity is given as the sum of the temperature independent residual resistivity  $\rho_{\text{def}}$  and due to phonon scattering  $\rho_{\text{ph}}(T)$ , which is temperature dependent.

$$\rho = \rho_{ph}(T) + \rho_{def}$$

The four-probe method is a simplest technique for resistivity measurements. In this technique four leads are attached to the sample surface (The rectangular shaped samples 10mm in length and 2mm in width were used) at equal distances. Generally silver paint contacts (with low contact resistance) are used to attach the wires to the surface of the sample. A complete resistivity setup is shown in Fig.2.4. The resistivity is calculated by using the following formula.

$$\rho = \frac{V(T)A}{IL}$$

where,  $V(T)$  = Voltage drop across the sample,  $L$  = Length of the sample,  $I$  = Current through the sample, and  $A$  = Cross-sectional area of the sample.

A constant current source was used to supply the current to the sample across the outer leads and the potential difference is measured between the middle leads. A measuring current of 1 mA or 2 mA was applied during these measurements. A liquid nitrogen dewer was used as a cryostat for the measurement of temperature dependent resistivity. The resistivity measurements were carried out during the heating cycle from 77 K to room temperature.. The XY recorder VP-6424A from National was used to record the data.

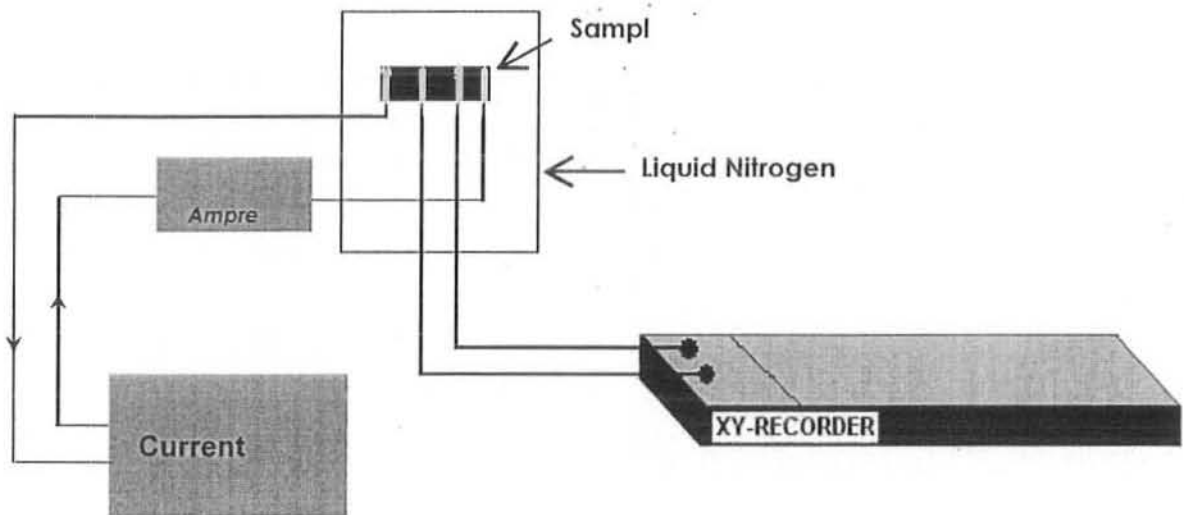


Fig. 2.4. Resistivity measurements setup.

### 2.3.4 Fourier transforms infrared spectroscopy

Atoms and molecules in a solid are in a continuous state of vibration even at absolute zero temperature. A molecule vibrates by bending, stretching, and contraction of the bonds joining the two atoms. Quantum mechanically the energy associated with these vibrations can be calculated by simple harmonic oscillator approximation

$$E_n = \left(n + \frac{1}{2}\right) \eta \omega_0$$

For  $n=0$ ,  $E_0 = \frac{1}{2} \eta \omega_0$  which shows that molecular vibrations have non-zero ground state energy. The Fourier Transform Infrared (FTIR) absorption spectroscopy is the most useful technique to detect these molecular vibrations and the spectrometer used for these measurements is called FTIR spectrometer. An FTIR spectrometer basically consists of a Michelson interferometer, which can separate the infrared radiations into its component wavelengths. A basic diagram of a Michelson interferometer is shown in Fig.2.5 and the schematic diagram of FTIR system is shown in Fig.2.6. The infrared radiations are used because the frequency of lattice vibrations lies in the range of infrared region of electromagnetic spectrum [6]. The infrared radiations interact with the molecular vibrations and if the natural frequency of vibration of a molecule matches with the frequency of infrared radiation then these radiations will be absorbed and an absorption peak associated with this particular vibrational mode will appear in the spectrum. All vibrations in a solid are not infrared active; only the vibrational modes, which produce a fluctuating dipole moment (Fluctuating dipole moments interact with the electric field of infrared radiations), are infrared active. The molecules of  $N_2$ ,  $O_2$ ,  $H_2$ , etc are infrared inactive because they don't have dipole moment. It is also observed that not all vibrational modes associated with a particular molecule are infrared active. In  $CO_2$  for example the symmetrical stretching or contraction does not produce an oscillating electric field and so these modes are not observed in an infrared spectrum. But asymmetrical stretching or contraction leads to fluctuating dipole moment and it can absorb the infrared radiations [7]. Fig.2.7 shows the vibrational modes of  $CO_2$  molecules. In oxide superconductors it may be possible that the electron-phonon

interaction is the origin of superconductivity in these compounds as in conventional superconductors. So the infrared absorption spectroscopy for the study of a possible connection between the lattice vibrations and the superconductivity is very useful. In these studies an FTIR spectrometer from Nicolet, was used. The bulk superconductor samples were studied. In the case of bulk samples, very thin pellets were made by mixing a small amount of the sample with KBr. The background spectrum was taken with KBr pellet and then the sample spectrum was observed. The numbers of scans taken for the background and sample spectrum were 10 and 50 respectively. The spectrometer subtracts the background spectrum and the final absorption spectrum of the sample is obtained. The resolution of the spectrometer was set in the spectral rang of  $400\text{-}700\text{ cm}^{-1}$ . The spectrometer was always purged with nitrogen gas before taking any absorption spectrum. The resulted spectra were interpreted by using the lattice dynamical calculations of the optical modes of vibrations in high temperature superconductors. The lattice dynamical data is helpful in assigning vibrational modes to a particular atom in the superconductor samples.

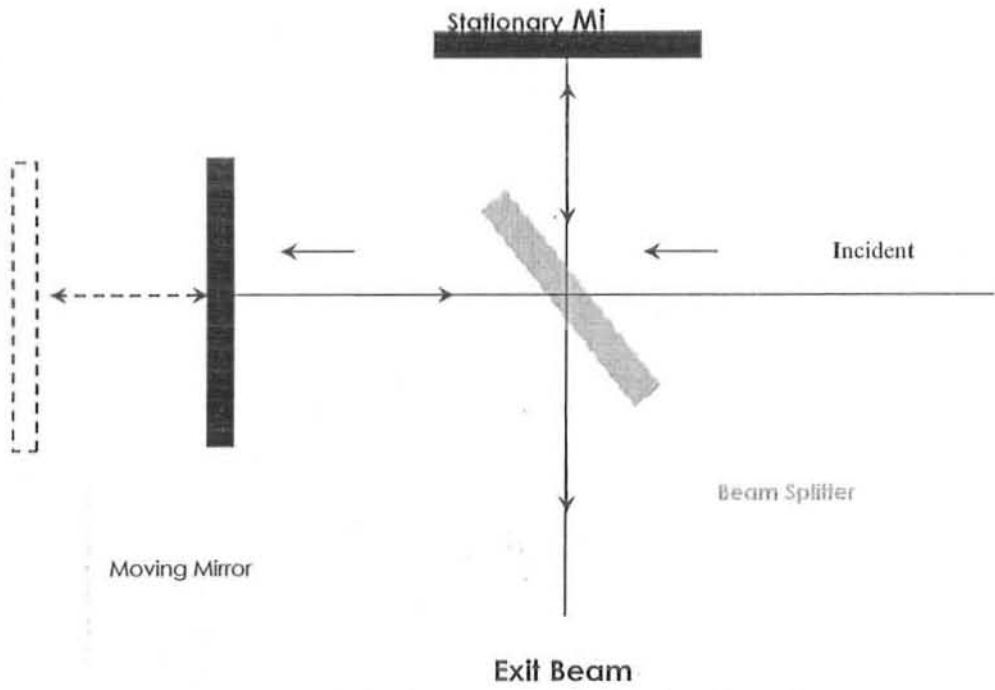


Fig. 2.5 A basic diagram of a Michelson interferometer

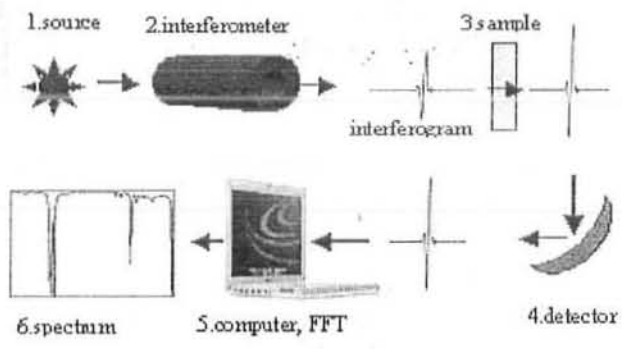


Fig. 2.6 A schematic diagram of FTIR system

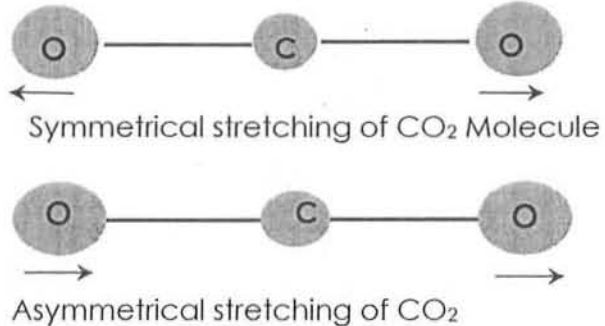


Fig. 2.7 Vibrational modes of CO<sub>2</sub> molecules.

## References:

- [1] H. London, Proc. Roy. Soc. A, **176**, 522(1940).
- [2] *Element of X-ray Diffraction*, B. D Cullity, Adison-Wesley, Second edition (1978).
- [3] *Condensed Matter Physics* M. P Marder, John Wiley & Sons Inc, **58** (2002).
- [4] Martin Nikolo, Am, J. Phys. **63**,1(1995).
- [5] *Solid State Physics: An Introduction to Theory and Experiment* Harald Ibach, and Hans Luth, (Springer-Verleg, 1991).
- [6] *Fourier Transform Infrared Spectroscopy*, P. R. Griffiths, (Jhon-Wiley, 1986).
- [7] *Spectroscopy*, V. B. Patania, Campus Books International, New Delhi (2002).

# Chapter#3

## Results and Discussion

### 3.1 Introduction

The existence of superconductivity in  $(\text{Cu}_{0.5}\text{Tl}_{0.5})\text{Ba}_2\text{Ca}_{n-1}\text{Zn}_n\text{O}_{2n+4-\delta}$  ( $n=3,4$ ) superconductors with  $\text{ZnO}_2$  planes [1,2] is preferred over its parent compound  $(\text{Cu}_{0.5}\text{Tl}_{0.5})\text{Ba}_2\text{Ca}_{n-1}\text{Cu}_n\text{O}_{2n+4-\delta}$  ( $n=3,4$ ) with  $\text{CuO}_2$  [3,4], due to the fixed valance state of zinc which can introduce a material with uniform carrier density in the inner and outer planes. In the later compound existence of anti-ferromagnetism is witnessed in the inner  $\text{CuO}_2$  planes. The anti-ferromagnetic alignment of spins of  $3d^9$  Cu atoms is suggested to arise from the deficiency of the carriers there the outer planes and over-doped whereas the inner planes are under-doped with the carriers. The existence of anti-ferromagnetism in the IP of  $\text{MBa}_2\text{Ca}_{n-1}\text{Cu}_n\text{O}_{2n+4-\delta}$  ( $M=\text{Bi, Tl, Hg, Cu}$ ) superconductors has been found to suppress the critical temperature and magnitude of diamagnetism [5]. Another advantage a superconductor with  $\text{ZnO}_2$  planes with filled  $3d^{10}$  shell is suppression of local spin density which was being induces by Cu  $3d^9$  shell in the  $\text{CuO}_2$  planes and hence the interactions of spins with the free carriers in Zn-doped compounds is significantly reduced. It has also been observed from our studies that hundred percent Zn cannot replace the Cu atoms in  $(\text{Cu}_{0.5}\text{Tl}_{0.5})\text{Ba}_2\text{Ca}_{n-1}\text{Zn}_n\text{O}_{2n+4-\delta}$  ( $n=3,4$ ) and a solubility limit appears with 90% Zn doping at the Cu sites with the doping of Zn beyond this limit superconductivity disappears altogether. These observations lead us to a conclusion that some population of Cu  $3d^9$  atoms is essential in the  $\text{CuO}_2/\text{ZnO}_2$  planes for the accomplishment of charge transfer from the charge reservoir layer. Another suggestion arising out of these observations is existence of interactions of spin density wave with the charge density wave as proposed in the charge stripe model [6]. The ideal compound for such studies is two [7-13]  $\text{CuO}_2/\text{ZnO}_2$  planes plane  $\text{Cu}_{0.5}\text{Tl}_{0.5}\text{Ba}_2\text{Ca}_1\text{Cu}_{0.5}\text{Zn}_{1.5}\text{O}_{8-\delta}$  superconductor, because the under-doped inner-planes would be absent altogether in this compound.

In our previous studies we have develop a better correlation among the carriers in  $\text{ZnO}_2$  planes, by doping Mg at the Ca sites in  $(\text{Cu}_{0.5}\text{Tl}_{0.5})\text{Ba}_2\text{Ca}_{n-1}\text{Zn}_n\text{O}_{2n+4-\delta}$  ( $n=3,4$ ) superconductors,



consequently enhanced superconductivity is achieved. It was observed from the studies of the cell parameters of Mg doped compounds that volume of the unit cell decreases resulting in increase in the Fermi vector [ $K_F=(3\pi^2N/V)^{1/3}$ ], their coherence length [ $\xi_c=\hbar^2K_F/2m\Delta$ ] along c-axis and hence the Fermi velocity [ $V_F = \frac{\pi\xi_c\Delta}{\eta}$ ] of the carriers[15]. In the present experiments we have doped Be at the Ca sites in  $(\text{Cu}_{0.5}\text{Tl}_{0.5})\text{Ba}_2(\text{Ca}_{1-y}\text{Be}_y)(\text{Cu}_{0.5}\text{Zn}_{1.5})\text{O}_{8-\delta}$  ( $y=0, 0.15, 0.3, .45, 0.6, 0.75$ ) superconductors. The main objective of this to enhance the inter-plane coupling and increase the interactions of remaining Cu atoms spins with the carriers in the conducting  $\text{ZnO}_2/\text{CuO}_2$  planes. These experiments would help in understanding charge density wave and spin density wave and the role of their interaction in the mechanism of high temperature superconductivity.

### 3.2 Results and Discussion

The x-ray diffraction patterns of  $(\text{Cu}_{0.5}\text{Tl}_{0.5})\text{Ba}_2(\text{Ca}_{1-y}\text{Be}_y)(\text{Cu}_{0.5}\text{Zn}_{1.5})\text{O}_{8-\delta}$  ( $y=0, 0.15, 0.3, .45, 0.6$ ) [CuTl-1212] samples is shown in Fig3.1(a, b). These samples have shown a predominant single phase CuTl-1212 structure in which the c-axis length of the unit cell decreases with increased Be doping. The variation of cell parameters with Be doping is shown in Fig.3.2. A decrease in the c-axis length with the increased Be doping is reminiscent of enhanced inter-plane coupling which would increase the coherence length along c-axis. A decrease in the anisotropy [16-19] will promote a decrease in the mean free path of carriers and hence improve their conductivity along the c-axis. The decrease in the c-axis length may be due to the suppression of Jahn-Teller distortion [20, 21]. The  $\text{Cu}^{+2}$  ions exhibit a strong Jahn-Teller effect the octahedron around  $\text{Cu}^{+2}$  is elongated along c-axis whereas the octahedrons around  $\text{Zn}^{+2}$  are intact because  $\text{Zn}^{+2}$  is in the  $d^{10}$  state. Therefore, doping of Zn at Cu sites will reduce the local Jahn-Teller distortion, and hence reduces the c-axis length [22]. The substantial decrease in c-axes length with Zn substitution suppresses the volume of the unit cell and hence would increase the Fermi wave vector [ $K_F = (3\pi^2 \frac{N}{V})^{1/3}$ ] along the c-axis.

The increase in the  $K_F$ , would enhance the coherence length along c-axis ( $\xi_c = \frac{\eta K_F}{2m\Delta}$ ) and the Fermi velocity of the carriers ( $v_F = \frac{\pi\xi_c\Delta}{\eta}$ )  $v_F$  is the Fermi velocity of the carriers and  $\Delta$  is

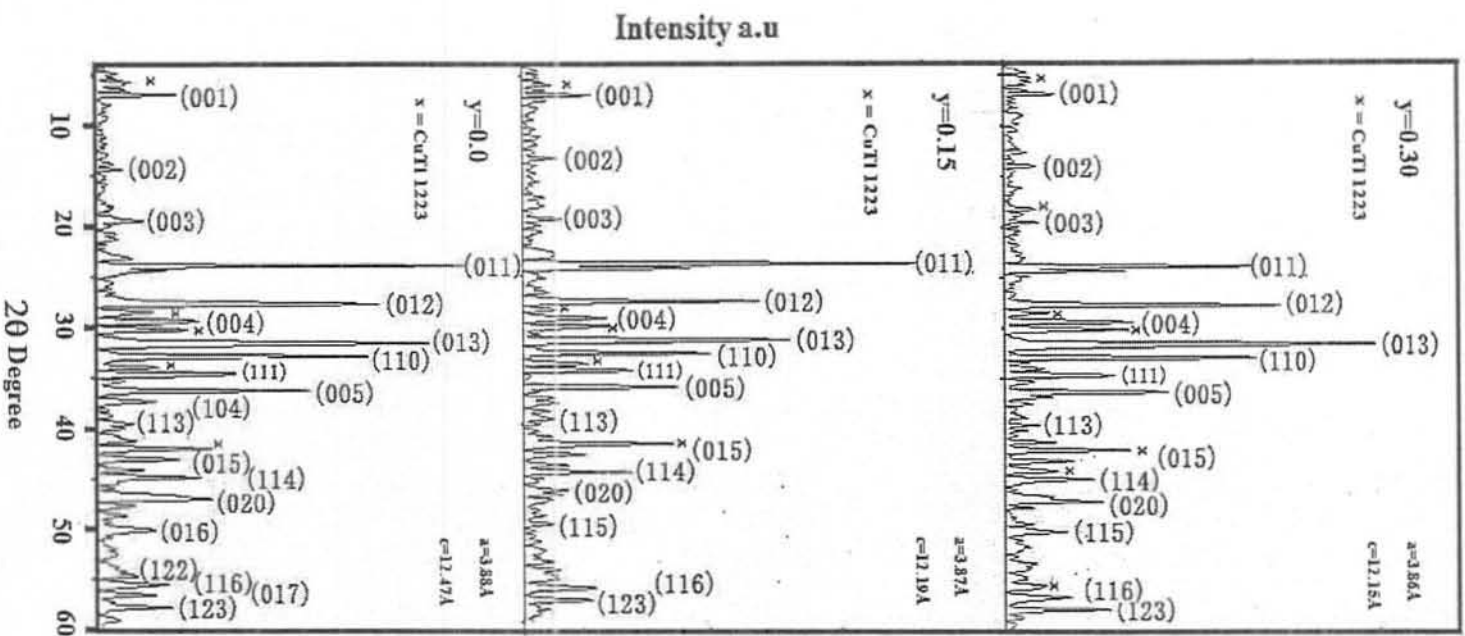


Fig.3.1 (a) X-ray diffraction ( $y=0.0, 0.15, 0.30$ ) Superconductors.

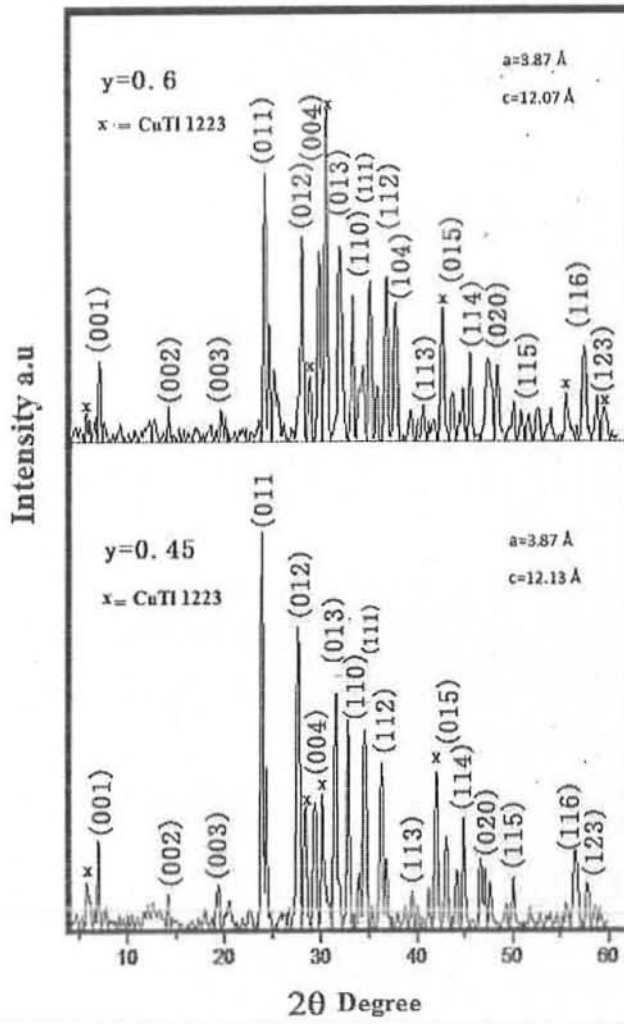


Fig.3.1 (b) X-ray diffraction ( $y= 0.45, 0.60$ ) Superconductors.

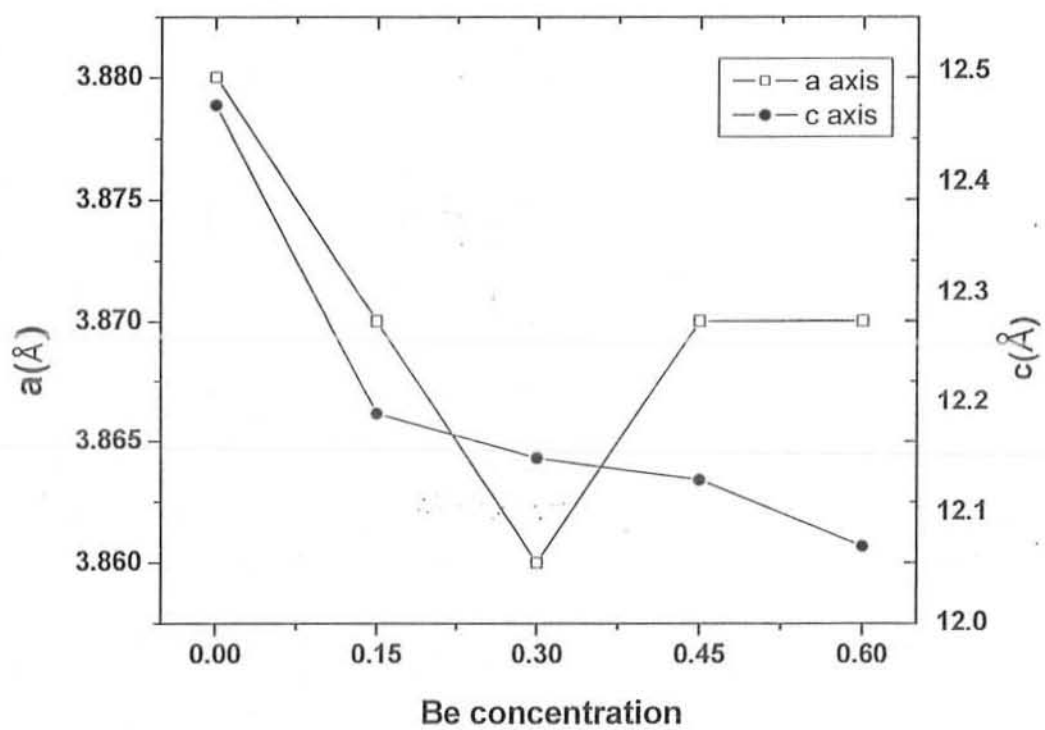


Fig.3.2. Variation of cell parameters v/s Be concentration

pairing potential. The increased Fermi velocity along c-axis would enhance the superconductivity parameters and 3D conductivity in the unit cell is improved. It is, therefore, the reduction of c-axis length which improves 3D conductivity and the homogeneous distribution of the carriers in the conducting  $\text{CuO}_2/\text{ZnO}_2$  planes. Interestingly, in the previous studies the decrease in c-axis length is correlated with the increase of  $T_c$  in Zn doped  $\text{Cu}_{0.5}\text{Tl}_{0.5}\text{Ba}_2\text{Ca}_{n-1}\text{Cu}_{n-y}\text{Zn}_y\text{O}_{2n+4-\delta}$  ( $n=3, 4$ ) superconductors.

$\text{Cu}_{0.5}\text{Tl}_{0.5}\text{Ba}_2\text{Ca}_{n-1}\text{Cu}_{n-y}\text{Zn}_y\text{O}_{2n+4-\delta}$  ( $n=3, 4$ ) high temperature superconductors [23,24 ], the apical oxygen phonon modes of type  $\text{Tl-O}_A\text{-M}(2)$  and  $\text{Cu}(1)\text{-O}_A\text{-Cu}(2)$  are observed in the wave number range  $400\text{-}480$  and  $480\text{-}530\text{cm}^{-1}$ . The  $\text{CuO}_2$  planar oxygen mode is observed around  $573\text{-}578\text{cm}^{-1}$ . The FTIR absorption measurements of  $(\text{Cu}_{0.5}\text{Tl}_{0.5})\text{Ba}_2(\text{Ca}_{1-y}\text{Be}_y)(\text{Cu}_{0.5}\text{Zn}_{1.5})\text{O}_{8-\delta}$  ( $y=0, 0.15, 0.3, 0.45, 0.6, 0.75$ ) samples are shown in Fig.3.3(a,b). The maximum of the  $\text{Tl-O}_A\text{-M}(2)$  band is observed around  $480\text{cm}^{-1}$  in  $\text{Cu}_{0.5}\text{Tl}_{0.5}\text{Ba}_2\text{Ca}_{n-1}\text{Cu}_{n-y}\text{Zn}_y\text{O}_{2n+4-\delta}$  ( $n=3, 4$ ) samples. whereas this band is peaked around  $462\text{-}465\text{cm}^{-1}$  in  $(\text{Cu}_{0.5}\text{Tl}_{0.5})\text{Ba}_2(\text{Ca}_{1-y}\text{Be}_y)(\text{Cu}_{0.5}\text{Zn}_{1.5})\text{O}_{8-\delta}$  ( $y=0, 0.15, 0.3, 0.45, 0.6, 0.75$ ) samples. The intensity of the apical oxygen mode of the type  $\text{Cu}(1)\text{-O}_A\text{-Cu}(2)/\text{Zn}$  around  $490\text{-}510\text{cm}^{-1}$  is increased with increased Be doping. The  $\text{CuO}_2$  planar mode remains around  $555\text{-}557\text{cm}^{-1}$  in Be undoped and Be doped samples. FTIR absorption measurements of oxygen post-annealed samples are shown in Fig. 3.3(c,d). Oxygen post-annealed samples have shown  $\text{Tl-O}_A\text{-M}(2)$  band peaked around  $462, 463, 465, 465, 465.5, 465\text{cm}^{-1}$  for the Be doping of  $0, 0.15, 0.3, 0.45, 0.6, 0.75$  in  $(\text{Cu}_{0.5}\text{Tl}_{0.5})\text{Ba}_2(\text{Ca}_{1-y}\text{Be}_y)(\text{Cu}_{0.5}\text{Zn}_{1.5})\text{O}_{8-\delta}$  samples. After post annealing in oxygen atmosphere, the intensity of apical oxygen mode of type  $\text{Cu}(1)\text{-O}_A\text{-Cu}(2)$  which is observed around  $491\text{-}509\text{cm}^{-1}$  is significantly increased with the increased Be-doping. The  $\text{CuO}_2/\text{ZnO}_2$  planar mode after post-annealing in oxygen atmosphere is observed around  $555\text{-}557\text{cm}^{-1}$  for all  $(\text{Cu}_{0.5}\text{Tl}_{0.5})\text{Ba}_2(\text{Ca}_{1-y}\text{Be}_y)(\text{Cu}_{0.5}\text{Zn}_{1.5})\text{O}_{8-\delta}$  ( $y=0, 0.15, 0.3, 0.45, 0.6, 0.75$ ) samples. It could be seen from the assignment of FTIR absorption modes that apical oxygen and  $\text{CuO}_2/\text{ZnO}_2$  planar modes stay unchanged in as-prepared and oxygen post-annealed samples, showing that equivalent crystallographic  $\text{CuO}_2/\text{ZnO}_2$  planes are optimally doped with the carriers and Be doping do not significantly modify the polarizability of various vibration bands. It is most likely that due to the uniform and optimal doping of the carriers in the equivalent  $\text{CuO}_2/\text{ZnO}_2$  planes, the anti-ferromagnetic order of the spins in the planes is absent altogether.

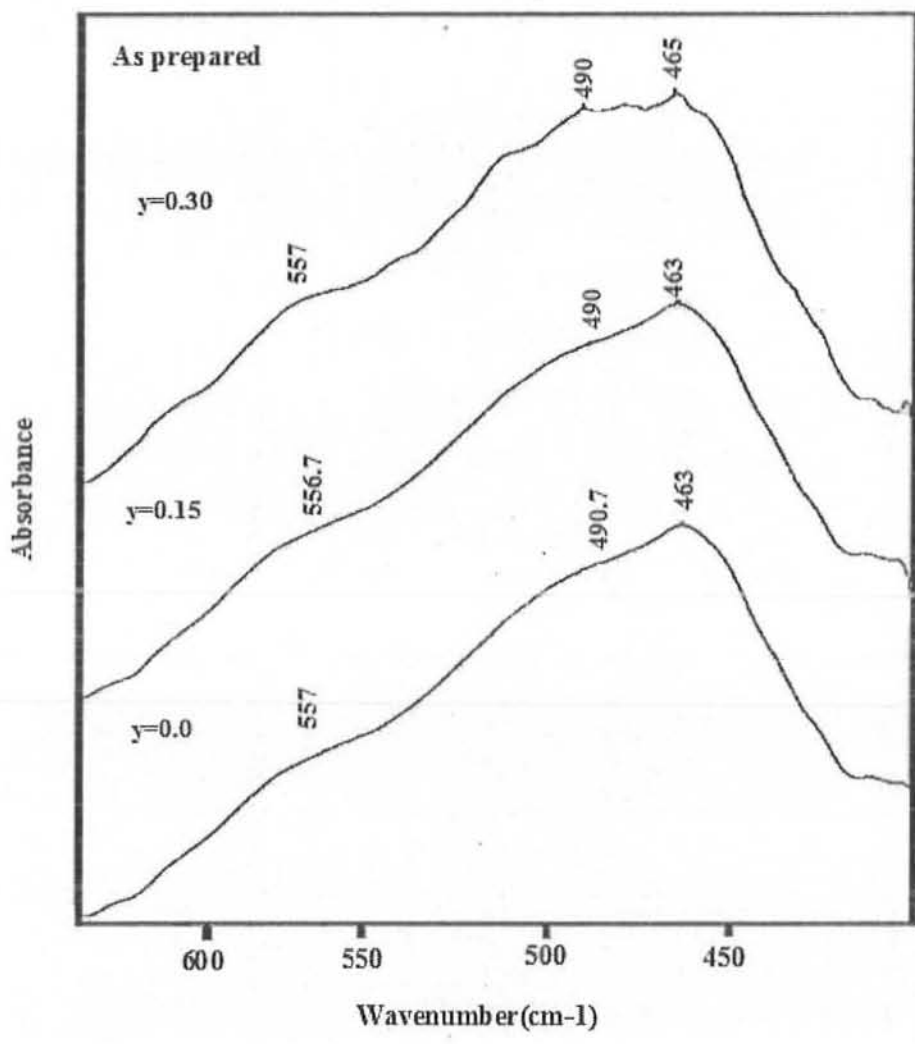


Fig.3.3 (a). Infrared absorption spectra of ( $y=0.0, 0.15, 0.30$ ) Superconductor.

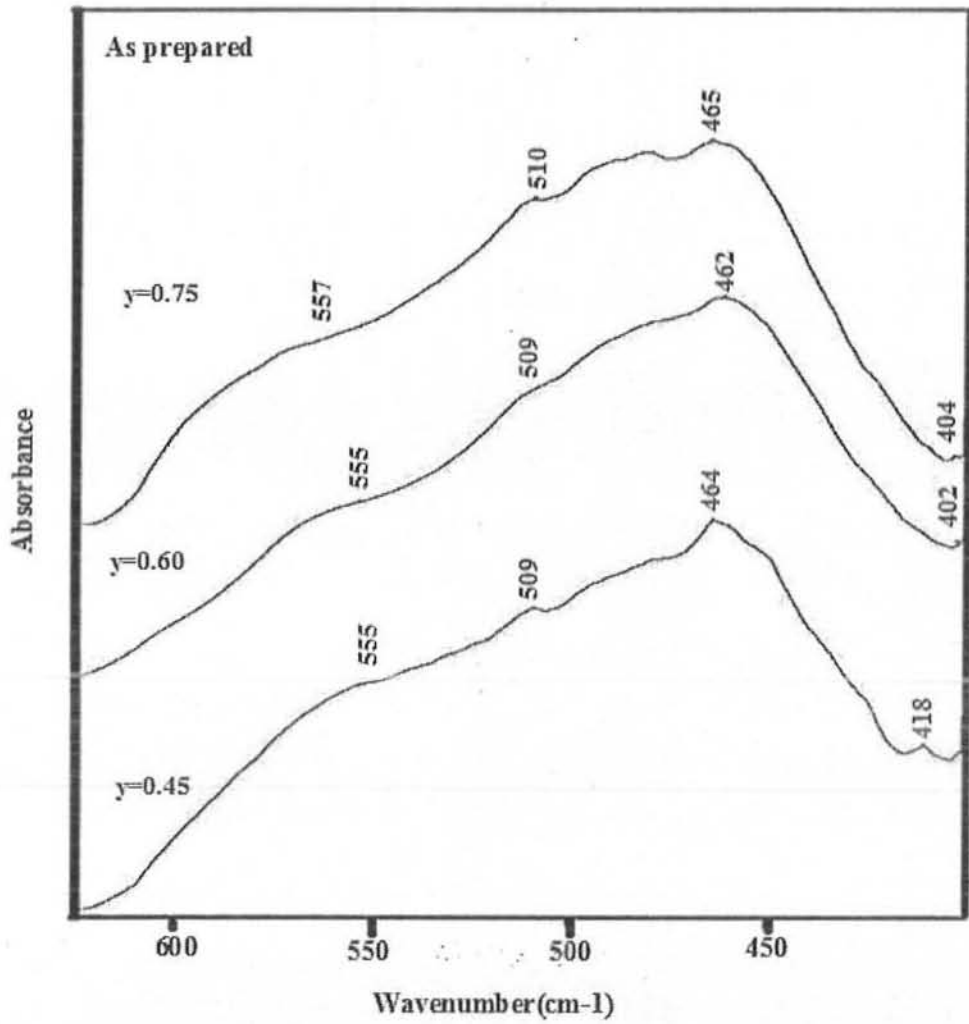


Fig.3.3(b). Infrared absorption spectra of ( $y=0.45, 0.60, 0.75$ ) Superconductor.

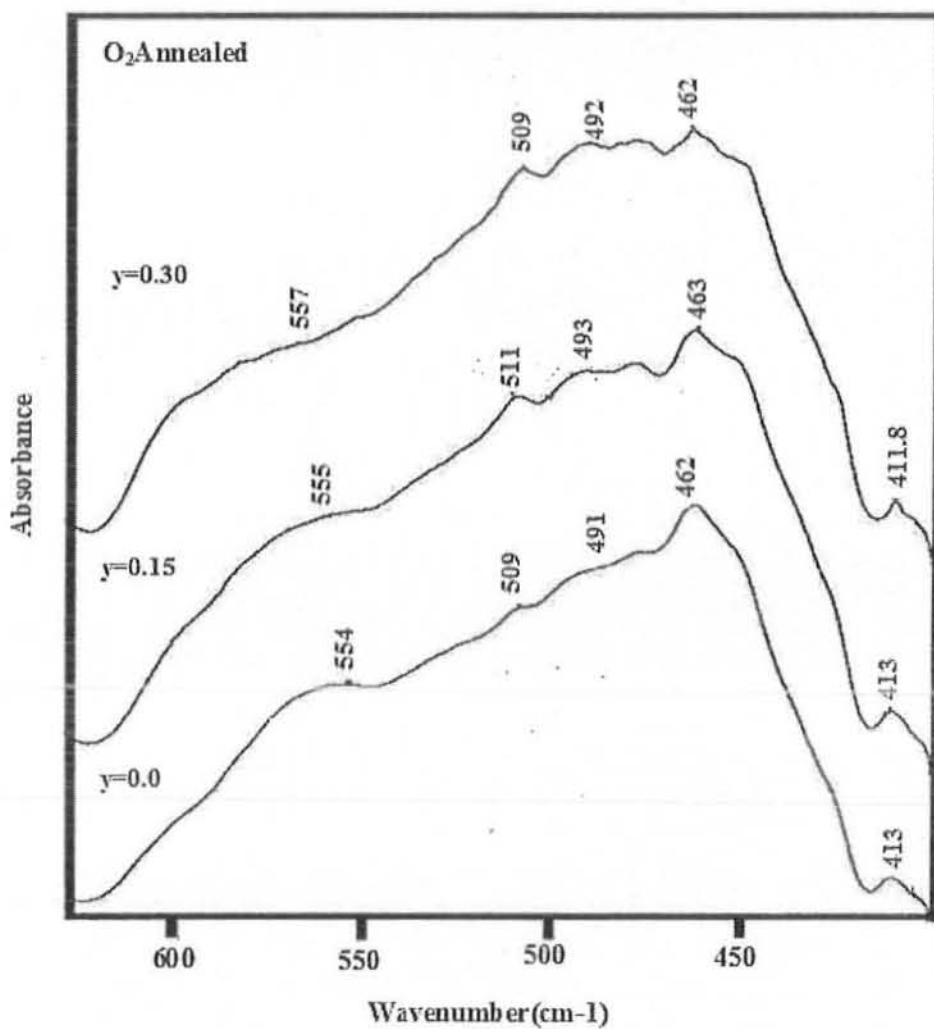


Fig.3.3(c) Oxygen-annealed infrared absorption spectra of ( $y=0.0, 0.15, 0.30$ ) Superconductor.



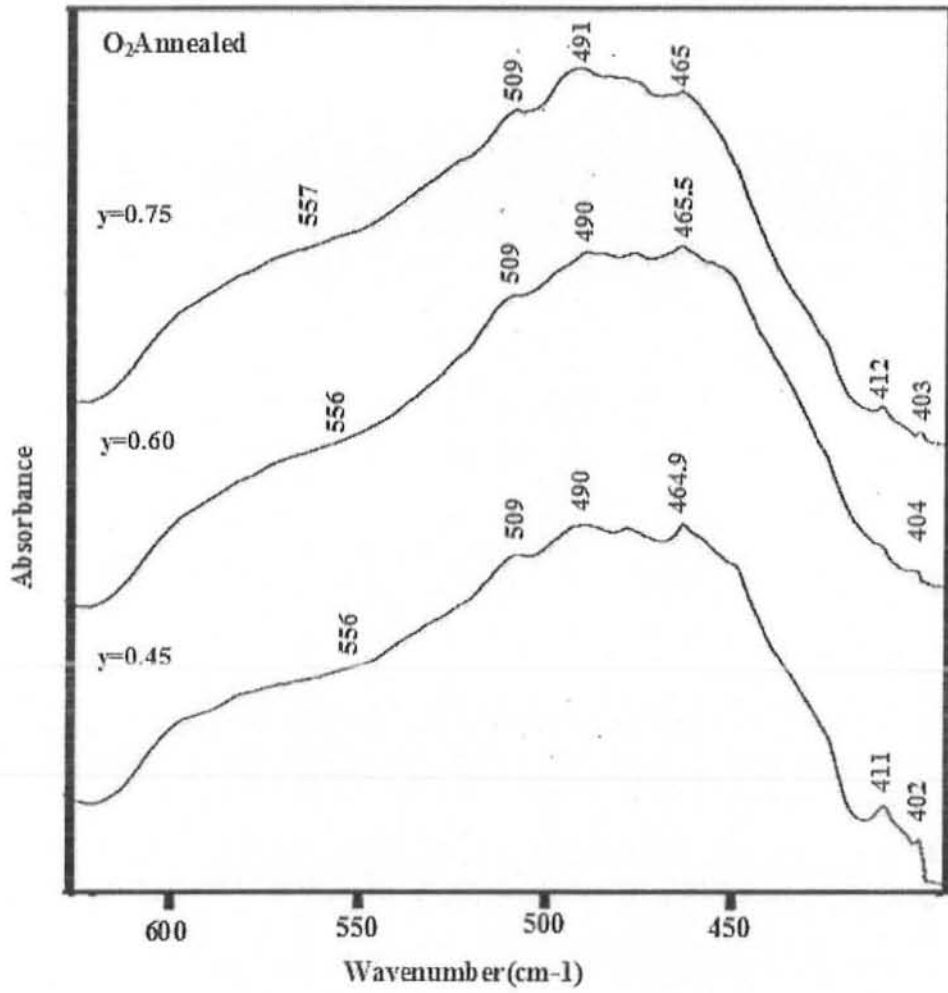


Fig.3.3(d) Oxygen-annealed infrared absorption spectra of (y=0.45, 0.60, 0.75) Superconductor.

The resistivity variations as function of temperature in  $(\text{Cu}_{0.5}\text{Tl}_{0.5})\text{Ba}_2(\text{Ca}_{1-y}\text{Be}_y)(\text{Cu}_{0.5}\text{Zn}_{1.5})\text{O}_{8-\delta}$  ( $y=0, 0.15, 0.3, 0.45, 0.6$ ) samples are shown in Fig.3.4(a,b). A metallic variation of resistivity from room temperature down to onset of superconductivity is salient feature of all the samples. These samples have shown onset of superconductivity around 112, 114.3, 108, 111, 106K and  $T_c(R=0)$  around 95.4, 89.2, 94.4, 98, 91K. The resistivity measurements of oxygen post-annealed samples are shown in Fig.3.5(a,b). The normal state resistivity of all the oxygen annealed samples is decreased almost to one half of its value observed in the un-annealed samples. Oxygen post-annealed samples have shown onset of superconductivity around 104.4, 103, 96, 101.4, 100K and zero-resistivity critical temperature around 100, 94.4, 87, 95, 93.4K, respectively. The resistivity measurements of as-prepared and oxygen post-annealed  $(\text{Cu}_{0.5}\text{Tl}_{0.5})\text{Ba}_2(\text{Ca}_{0.25}\text{Be}_{0.75})(\text{Cu}_{0.5}\text{Zn}_{1.5})\text{O}_{8-\delta}$  [i.e the samples with  $y=0.75$ ] are shown in Fig.3.7. The as-prepared  $(\text{Cu}_{0.5}\text{Tl}_{0.5})\text{Ba}_2(\text{Ca}_{0.25}\text{Be}_{0.75})(\text{Cu}_{0.5}\text{Zn}_{1.5})\text{O}_{8-\delta}$  samples have shown metallic variations from room temperature down to onset of superconductivity around 103K, but  $T_c(R=0)$  is not achieved down to 77K. After post-annealing oxygen atmosphere, the onset of superconductivity is decreased to 101K, however, the transition to the superconductivity became sharp. It is most likely that Be doping of  $y=0.75$  is the solubility limit of Be in  $(\text{Cu}_{0.5}\text{Tl}_{0.5})\text{Ba}_2(\text{Ca}_{1.25}\text{Be}_{0.75})(\text{Cu}_{0.5}\text{Zn}_{1.5})\text{O}_{8-\delta}$  system. The variation of  $T_c$  with Be concentration of as prepared and  $\text{O}_2$  annealed sample as shown in fig 3.6(a,b).

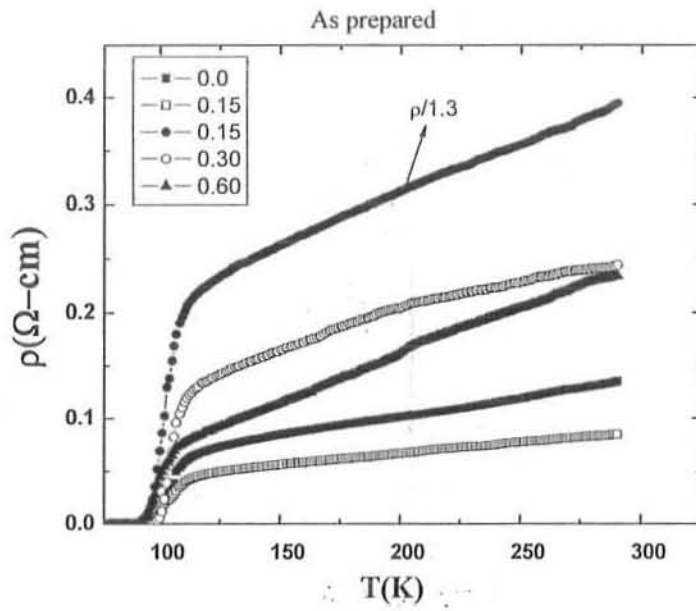


Fig.3.4a. Resistivity v/s Temperature graph of as prepared samples.

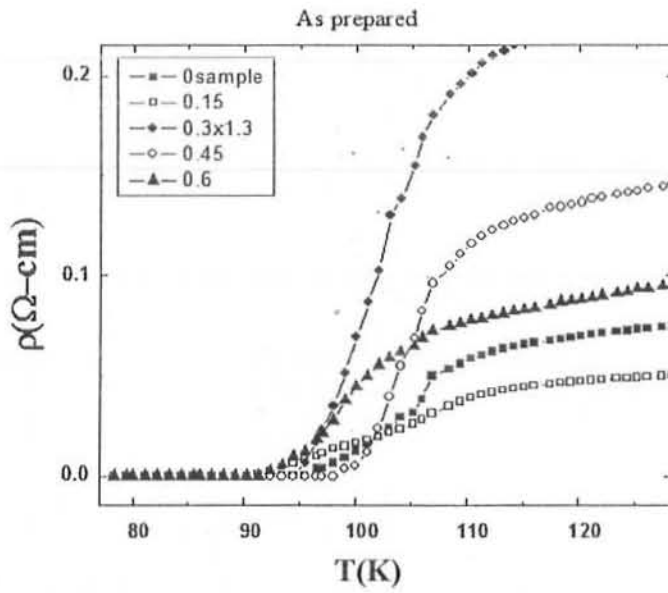


Fig3.4b. Transition region of the samples  $y=0.0, 0.15, 0.30, 0.45, 0.60$

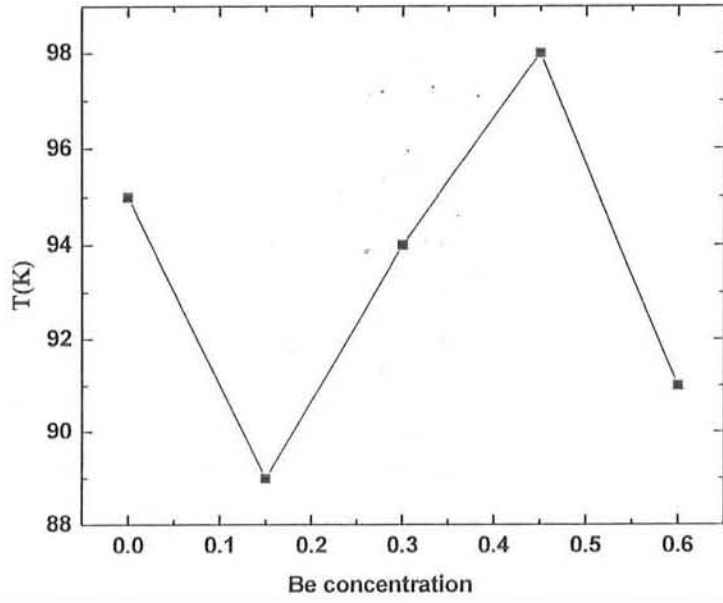


Fig3.6(a). Tc v/s Be concentration of as prepared samples.

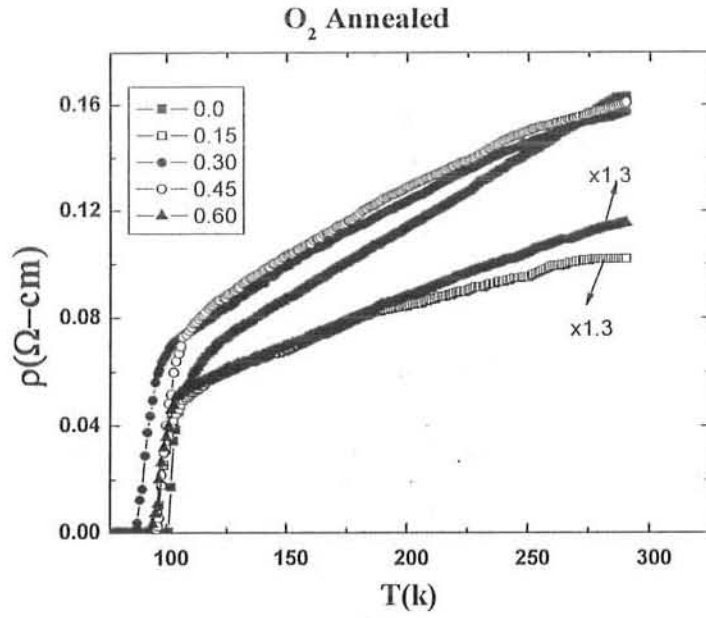


Fig.3.5a Resistivity v/s Temperature plot of Oxygen- annealed samples.

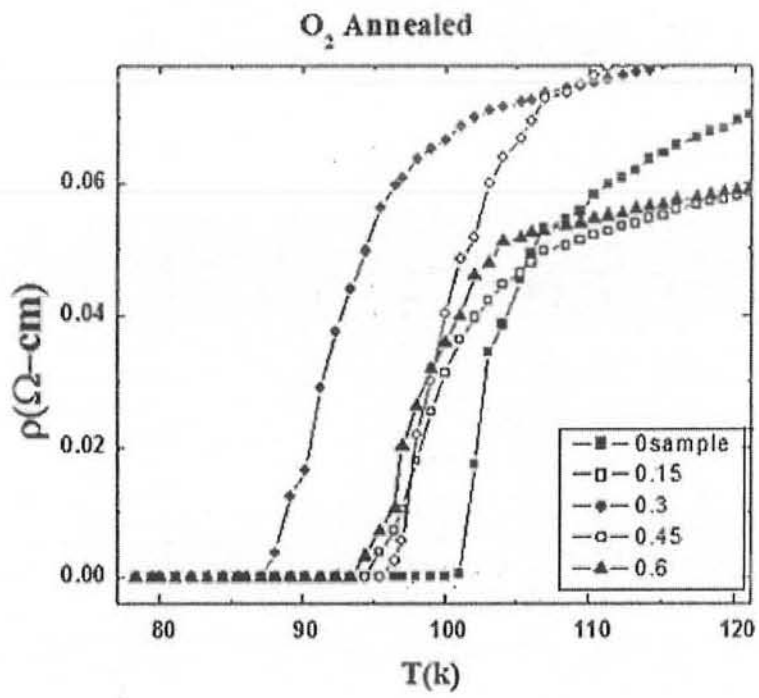


Fig3.5b Transition regions of the  $O_2$  annealed samples.

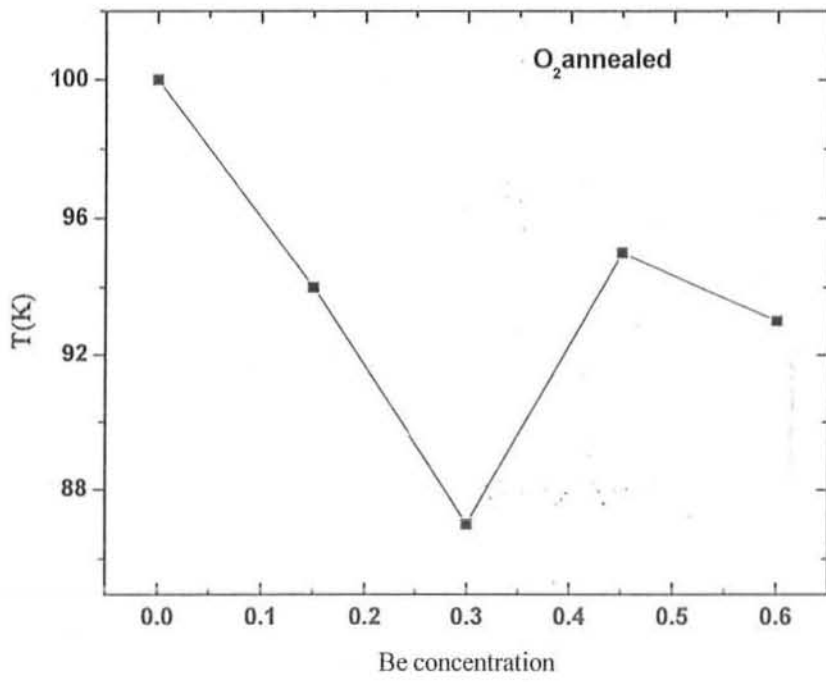


Fig3.6 (b) Variation of  $T_c$  with Be concentration  $O_2$  annealed samples.

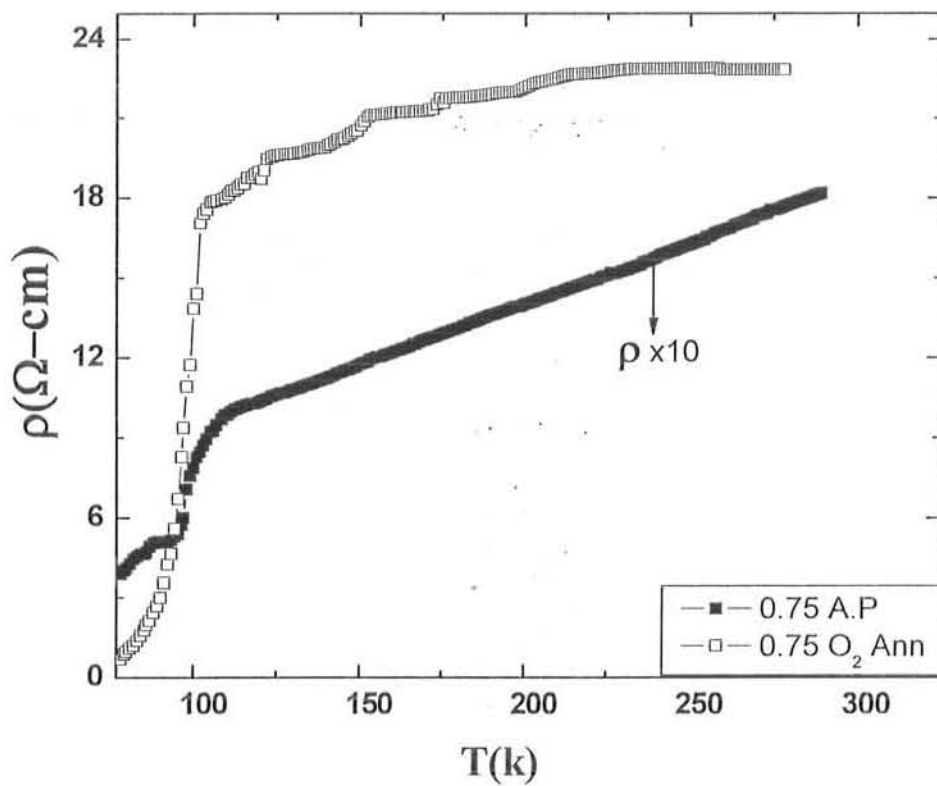


Fig.3.7 Resistivity of as prepared and O<sub>2</sub> Annealed sample  $y=0.75$

Diamagnetic measurements of as-prepared  $(\text{Cu}_{0.5}\text{Tl}_{0.5})\text{Ba}_2(\text{Ca}_{1-y}\text{Be}_y)(\text{Cu}_{0.5}\text{Zn}_{1.5})\text{O}_{8-\delta}$  ( $y=0, 0.15, 0.3, 0.45, 0.6$ ) samples are shown in Fig.3.8a. In comparison with Be un-doped samples, the magnitude of diamagnetism decreases in the samples with increasing Be concentration.  $(\text{Cu}_{0.5}\text{Tl}_{0.5})\text{Ba}_2(\text{Ca}_{1-y}\text{Be}_y)(\text{Cu}_{0.5}\text{Zn}_{1.5})\text{O}_{8-\delta}$  ( $y=0, 0.15, 0.3, 0.45, 0.6$ ) samples have shown onset of superconductivity in the in-phase component of magnetic susceptibility around 110, 111, 109, 112, 110K and the peak temperature in the out-of-phase component of susceptibility around 109, 104, 92, 93, 96K, respectively. The ac-susceptibility measurements of oxygen post-annealed samples are shown in Fig.3.8b.  $(\text{Cu}_{0.5}\text{Tl}_{0.5})\text{Ba}_2(\text{Ca}_{1-y}\text{Be}_y)(\text{Cu}_{0.5}\text{Zn}_{1.5})\text{O}_{8-\delta}$  ( $y=0, 0.15, 0.3, 0.45, 0.6$ ) samples have shown onset of superconductivity in the in-phase component of magnetic susceptibility around 110, 105, 113, 104, 103K and the peak temperature in the out-of-phase component of susceptibility around 101, 102, 110, 97, 93K, respectively. The magnitude of diamagnetism increases in samples with Be doping of  $y=0.3, .45, 0.6$ . In comparison with Be un-doped  $(\text{Cu}_{0.5}\text{Tl}_{0.5})\text{Ba}_2(\text{Ca}_1)(\text{Cu}_{0.5}\text{Zn}_{1.5})\text{O}_{8-\delta}$  samples, the magnitude of diamagnetism in Be doped  $(\text{Cu}_{0.5}\text{Tl}_{0.5})\text{Ba}_2(\text{Ca}_{1-y}\text{Be}_y)(\text{Cu}_{0.5}\text{Zn}_{1.5})\text{O}_{8-\delta}$  ( $y= 0.15, 0.3, 0.45$ ) samples increases whereas decreased in the  $(\text{Cu}_{0.5}\text{Tl}_{0.5})\text{Ba}_2(\text{Ca}_{0.4}\text{Be}_{0.6})(\text{Cu}_{0.5}\text{Zn}_{1.5})\text{O}_{8-\delta}$  [i.e samples with Be doping of  $y=0.6$ ]. The increased magnitude of diamagnetism is most likely arising from the optimization of the carriers in conducting  $\text{CuO}_2/\text{ZnO}_2$  planes. A summary of onset of superconductivity  $T_c(\text{onset})$  and  $T_c(\text{R}=0)$  in the resistivity measurements, and the onset of diamagnetism in the in-phase component of magnetic susceptibility and the peak temperature in the out-of-phase component, is given in Table1.



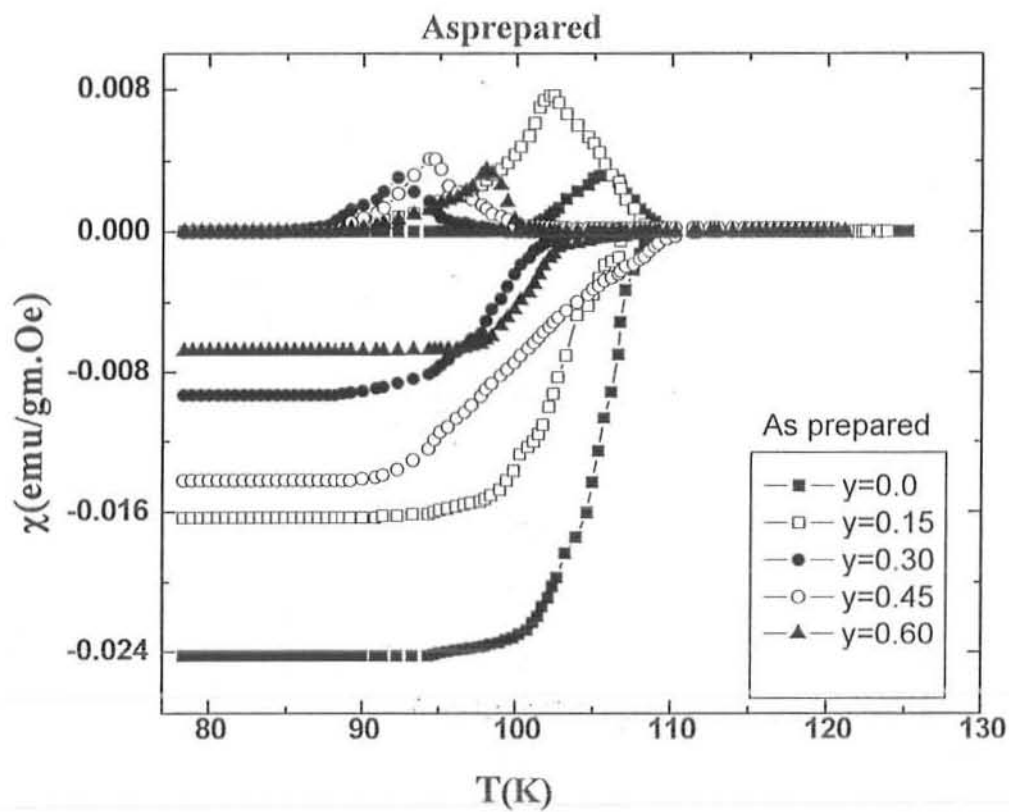


Fig.3.8(a) AC-susceptibility measurements versus temperature.

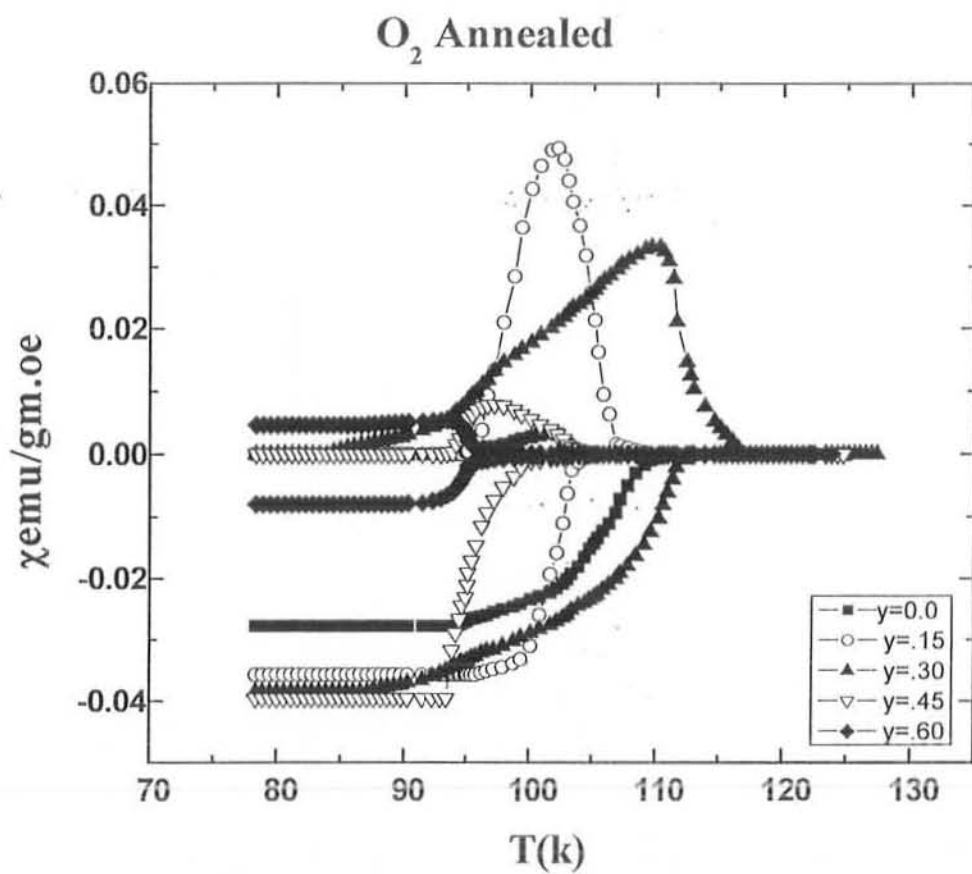


Fig.3.8(b) Oxygen-annealed AC-susceptibility measurements.

**Table .1.** A summary of onset of superconductivity  $T_c(\text{onset})$   $T_c (R=0)$  in resistivity measurements and the onset of diamagnetism in In phase component of magnetic susceptibility and peak temperature in out phase component. Where x shows no zero resistance state.

Y	AS PREPARED				O <sub>2</sub> ANNEALED			
	$T_c(R=0)$	$T_c$ onset(K)	$T_p$ (K)	$\chi_{on}$ (K)	$T_c(R=0)$	$T_c$ onset(K)	$T_p$ (K)	$\chi_{on}$ (K)
0.0	95	112	109	110	100	104	101	110
0.15	89	114	104	111	94	103	102	105
0.30	94	108	92	109	87	96	110	113
0.45	98	111	93	112	95	101	97	104
0.60	91	106	96	110	93	100	93	103
0.75	X	103	X	X	X	101	X	X

### 3.3 Conclusion

In conclusion we have successfully synthesized Be doped  $(\text{Cu}_{0.5}\text{Tl}_{0.5})\text{Ba}_2(\text{Ca}_{1-y}\text{Be}_y)(\text{Cu}_{0.5}\text{Zn}_{1.5})\text{O}_{8-\delta}$  ( $y=0.0, 0.15, 0.3, 0.45, 0.6$ ) superconductors at normal pressure. This system is iso-structural to YBaCuO oxide in which the carrier's concentration is highly susceptible to the oxygen contents in the charge reservoir layer. In YBaCuO system the planes are separated by Ca atoms, whereas in our  $(\text{Cu}_{0.5}\text{Tl}_{0.5})\text{Ba}_2(\text{Ca}_{1-y}\text{Be}_y)(\text{Cu}_{0.5}\text{Zn}_{1.5})\text{O}_{8-\delta}$  system the  $\text{CuO}_2/\text{ZnO}_2$  planes are separated by Ca atoms. The doping of Ca at the Y sites in YBaCuO suppress the critical temperature whereas incorporation of Be at the Ca sites in our  $(\text{Cu}_{0.5}\text{Tl}_{0.5})\text{Ba}_2(\text{Ca}_{1-y}\text{Be}_y)(\text{Cu}_{0.5}\text{Zn}_{1.5})\text{O}_{8-\delta}$  ( $y=0, 0.15, 0.3, 0.45, 0.6$ ) superconductors do not significantly suppress the critical temperature of the final compound. Not only this compound had higher zero resistivity critical temperature than YBaCuO but the magnitude of diamagnetism in  $(\text{Cu}_{0.5}\text{Tl}_{0.5})\text{Ba}_2(\text{Ca}_{1-y}\text{Be}_y)(\text{Cu}_{0.5}\text{Zn}_{1.5})\text{O}_{8-\delta}$  ( $y=0, 0.15, 0.3, 0.45$ ) superconductors is increased after optimization of the carriers. The decreased c-axis length is observed with the increased incorporation of Be showing enhanced inter-plane couplings in final compound. The positions of phonon bands related to apical oxygen atoms and  $\text{CuO}_2/\text{ZnO}_2$  planes are not significantly altered in all  $(\text{Cu}_{0.5}\text{Tl}_{0.5})\text{Ba}_2(\text{Ca}_{1-y}\text{Be}_y)(\text{Cu}_{0.5}\text{Zn}_{1.5})\text{O}_{8-\delta}$  samples showing that equivalent crystallographic  $\text{CuO}_2/\text{ZnO}_2$  planes are optimally doped with the carriers. Since the carrier's is not significantly altered, therefore, anti-ferromagnetic alignment of the spin arrangement in the conducting planes is absent altogether in  $(\text{Cu}_{0.5}\text{Tl}_{0.5})\text{Ba}_2(\text{Ca}_{1-y}\text{Be}_y)(\text{Cu}_{0.5}\text{Zn}_{1.5})\text{O}_{8-\delta}$  ( $y=0, 0.15, 0.3, 0.45, 0.6$ ) superconductors.

## References

- [1] B. A. Scott, E. Y. Suard, C. C. Tsuei, D. B. Mitzi, T. R. McGuire, B. -H. Chen, and D. Walker, *Physica C* **230** 239(1994).
- [2] E. V. Antipov, A. M. Abakumov, and S. N. Putilin, *Supercond. Sci. Technol.* **15** R31 R31. (2002).
- [3] M. Núñez-Regueiro, and C. Acha, *Studies on High  $T_c$  Superconductors*, Vol. **24**, Nova Science, Commack, NY, 2000.
- [4] M. -H. Julien, P. Carretta, M. Horvatic, C. Berthier, Y. Berthier, P. Segransan, A. Carrington, and D. Colson, *Phys. Rev. Lett.* **76** 4238. 4238(1996).
- [5] Y. Tokunaga, K. Ishida, Y. Kitaoka, K. Asayama, K. Tokiwa, A. Iyo and H. Ihara, *Phys. Rev. B* **61**, 9707 (2000).
- [6] O. Zachar, S. A. Kivelson, and V.J. Emery, *Phys. Rev. B* **57**, 1422 (1998).
- [7] A.Ehmann, S.Kemmler-sack, S.Losch, M.Schilichenmaier.W.Wischert, P.Zoller, T.Nissel and R.P.Huebener, *Physica C* **1981-6** (1992).
- [8] O.Chmaisem, L.Wessels, Z.Z.Sheng *Physica C* **228** 190-194 (1994).
- [9] G.C.Che, F.Wu, Y.C.Lan,H.Chen, C.Dong, B.Yin, S.L.Jia, Z.X.Zhao, *Physica C* **251** 110-114 (1995).
- [10] A.Kharlanov, J.P.Attfield *Physica C* **265** 315-322 (1996).
- [11] V.Badri, Y.T.Wang, J.Onstad and A.M.Hermann *Journal of Superconductivity*. Vol.**10**.No.5 1997.
- [12] P.Haldar, S.Sridhar, A.Roig-Janicki, W.Keeneady, D.H.Wu, C.Zahopoulos, and B.C.Giessen, *Journal of Superconductivity*, Vol.**1**, No.2,(1998).
- [13] G.C.Che, G.D.Lin, F.Wu, H.Chin, S.L.Jia, C.Dong and Z.X.Zhao, *Physica C* **341-348** 391-394 (2000).
- [14] G.Gritzner, H.Sudra and M.Eder, *Journal of Physics: Conference Series* **43** 462-465 (2006).
- [15] *Solid State Physics: An introduction to Theory and Experiment*, H. Ibach, H. Luth, first ed, Springer Velag, Berlin, 1993.
- [16] H. Ihara, *Physica C*, **289** 364-365 (2001).